2011

Comparison of TLD dose and reconstructed dose for post-mastectomy radiation therapy with TomoTherapy

Matthew Roberts
Louisiana State University and Agricultural and Mechanical College

COMPARISON OF TLD DOSE AND RECONSTRUCTED DOSE FOR POST-MASTECTOMY RADIATION THERAPY WITH TOMOTHERAPY

A Thesis

Submitted to the Graduate Faculty of the
Louisiana State University and
Agricultural and Mechanical College
in partial fulfillment of the
requirements for the Degree of
Master of Science

in

The Department of Physics and Astronomy

by
Matthew Thomas Roberts
B.A., Coe College, 2008
December 2011

Acknowledgements

I would like to thank my advisor, Dr. Brent Parker, for his support and guidance throughout this project. I also thank the members of my advisory committee: Dr. John Gibbons, Dr. Michael Price, Dr. Mary Ella Sanders, and Dr. Phillip Sprunger for their assistance and time in serving on this committee.

Several members of the Mary Bird Perkins Cancer Center team were instrumental in conducting this work, including Ricky Hesston for his help with much of the TomoTherapy software that was used; Layton Olano for assisting with the technical aspects of the TomoTherapy treatment machine; and Frank Apollo and Chad Dunn for their help in the treatment planning aspects of the project.

I would also like to thank Quan Chen and Geoff Sobering, members of TomoTherapy's research and development team, for their collaborations and assistance with software updates on the TomoTherapy research computer system.

Finally, I would like to thank the LSU Medical Physics Program and MBPCC for the use of offices and equipment throughout my time in the program and for providing me with an excellent graduate education.

Table of Contents

List of Tables

List of Figures

Abstract

Purpose: To determine the dosimetric accuracy of TomoTherapy's database technique for delivery verification and dose reconstruction in post-mastectomy radiation therapy (PMRT) treatments.

Methods and Materials: Archived treatment data for 5 patients treated at MBPCC were restored to the TomoTherapy research computer system. Pretreatment MVCT images and exit detector dosimetry data collected during treatment of these patients were used to calculate the DV sinogram for each treatment fraction. The DV sinogram and MVCT image for each fraction were used to reconstruct the delivered dose for that fraction using a convolution/superposition algorithm. The reconstructed doses were compared to previously acquired TLD doses for each patient. To supplement the results from the retrospective patient data comparison, and to reduce the variables involved in a patient treatment, a PMRT treatment was created for the RANDO phantom. Measured TLD doses were compared to reconstructed doses computed from the DV sinogram and MVCT images as well as reconstructed doses from the DV sinogram and kVCT images.

Results: The mean difference for all the patient data was -3.2 ± 4.7%. Approximately 66% of the data points agreed within 5%. The largest difference between measured and calculated doses was -17.3%. The mean difference for the phantom data for DV doses calculated from MVCT was 3.9 ± 2.6%. The largest difference between measured and calculated doses was 9.0%. Approximately 63% of the data points agreed within 5%. The mean difference for the phantom data for DV doses calculated from kVCT was 0.6 ± 2.9%. The largest difference

between measured and calculated doses was 5.4%. Approximately 88% of the data points agreed within 5%.

Conclusion: Patient motion was removed in the phantom study and there was still a large number of data points outside 5% for the DV doses calculated with MVCT. The DV doses calculated with kVCT had better agreement which indicates an inaccurate IVDT was used in the MVCT dose calculations. Discrepancies between TLD and reconstructed doses may be a result of the several problems including the inherent relatively large uncertainty of TLD, IVDT inaccuracies, and limitations of the database technique calculations near the surface.

Chapter 1. Introduction

I. Background and Significance

A. Post-Mastectomy Radiation Therapy

1) Indications

According to Surveillance Epidemiology and End Results (SEER) data from the National Cancer Institute (NCI), it is estimated that approximately 210,000 women in the United States will be diagnosed with invasive breast cancer annually. As many as 50% of these women may end up being treated with mastectomy [1].

After undergoing a modified radical mastectomy for invasive breast cancer, some of the cancer cells may be left behind and can lead to local recurrence of the tumor if they are not destroyed. One way of destroying these cells is by using radiation soon after undergoing a mastectomy. Post-mastectomy radiation therapy (PMRT) involves the use of radiation to treat the chest wall as well as the corresponding regional lymph nodes including the axillary, supraclavicular, and internal mammary nodes (Figure 1-1).

A study by Dewar et al. has shown that PMRT can decrease local recurrence by up to two thirds [2]. According to Recht et al., PMRT has also been shown to decrease the occurrence of developing distant metastases from the cancer cells traveling through the lymphatic system [3]. The combination of these two factors has shown an increase in the overall 10 year disease free survival of patients by 10% [4, 5].

Based on the results of several studies, a consensus panel of experts for the National Institute of Health (NIH) recommended the practice of PMRT for patients who are at a high risk of local recurrence. This panel classified patients as being at a high risk based on the following

indications: the presence of 4 or more positive lymph nodes or an advanced primary tumor (tumor size greater than or equal to 5 cm or a tumor invading the skin or adjacent musculature, i.e. T3 or T4 staged tumors) [6].

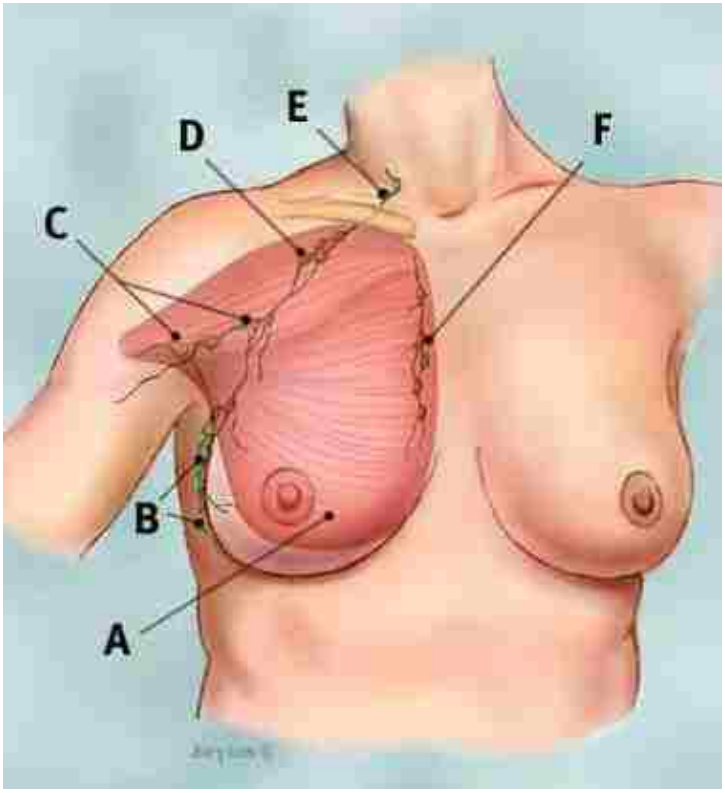

Figure 1-1: Diagram of chest wall showing locations of A – Pectoralis Major, B – Axillary Lymph Nodes (Level I), C – Axillary Lymph Nodes (Level II), D – Axillary Lymph Nodes (Level III), E – Supraclavicular Lymph Nodes, F – Internal Mammary Lymph Nodes [7]

At the time of the NIH recommendations it was uncertain whether or not PMRT should be used for patients with only 1 – 3 positive lymph nodes and T1 or T2 staged primary tumors. Since then, no other formal consensus recommendations have come out on the issue. However, more recent studies have shown that the largest survival benefits from PMRT do not occur in patients in the highest risk group of local recurrence [8], and instead other factors including age, estrogen receptor status, and the addition of hormone therapy may have a strong influence on

recurrence [9]. Local recurrence is a substantial clinical problem and has a significant impact on the outcome of patients with T1 or T2 primary tumors and 1 – 3 positive lymph nodes, and these patients may also benefit from PMRT and are encouraged to enter randomized trials that are currently ongoing [10]. MacDonald et al. suggest that for these intermediate risk patients, PMRT should be performed to only the chest wall and avoiding the regional lymphatics due to the fact that the greatest risk of recurrence is at the chest wall and additional radiation to the lymphatics increases the toxicity [11]. They show positive overall and disease free survival benefits through the use of this method. Since these patients are in the intermediate risk group where PMRT is a possibility, the choice often comes down to a combination of doctor, patient, and institution preferences.

2) Potential Risks

Although the potential benefits of PMRT seem quite clear there are still risks and challenges involved with its use. Sometimes treatment-related complications can occur that may cause problems for the patient after several years. Among these long term complications are lymphedema, cardiac toxicity, pulmonary fibrosis, brachial plexopathy, rib fractures, and secondary cancers [12].

Due to the fact that most of the patients undergoing PMRT will also be receiving systemic agents with cardiac and pulmonary toxicities of their own, extra care must be taken to avoid these structures with the toxicity of the radiation being delivered [13]. Most of the long term effects are relatively uncommon, but they are still of some concern due to the severe risks they pose to the patient. To avoid complications care must be taken to select the most effective planning target volumes (PTV) and treatment fields, as well as the proper treatment technique in order to destroy the cancer cells and spare healthy tissues at the same time [14].

3) Treatment Techniques

The proximity and arrangement of several vital dose limiting structures, including the heart and lungs, makes PMRT to the chest wall and regional lymph nodes challenging to plan and deliver. The goal of PMRT is to irradiate the chest wall and regional lymph nodes including the axillary, supraclavicular, and internal mammary nodes. Typical treatment doses are 1.8 – 2 Gy per fraction to a total of 50 – 50.4 Gy.

Of the traditional methods of treatment, there is no "gold standard". Each patient typically requires individualized treatment planning with complex field arrangements. Pierce et al. [15] compared seven of the most common treatment techniques (Figure 1-2) for treating the post-mastectomy chest wall along with the supraclavicular and internal mammary nodes. They found that none of the techniques they compared combined the best chest wall and regional node coverage with minimal lung and heart complication probabilities. However, of the seven techniques they studied, they supported partially wide tangent fields (PWTF) as the most appropriate balance of target coverage and normal tissue sparing. Although, based on the results of their work, each patient still requires careful individual planning and treatment selection because the PWTF may not be the best choice for every patient.

The application of intensity-modulated radiation therapy (IMRT) to treat the chest wall and regional lymph nodes for PMRT has been studied by Krueger et al. [13]. Their goal was to show that IMRT could achieve better target coverage while maintaining or improving sparing of nearby critical structures. In their study, they created 9-field IMRT plans designed to match the low heart doses of the PWTF technique of Pierce et al. while maintaining the same prescription to the chest wall, internal mammary nodes, and supraclavicular nodes. Normal tissue doses were then minimized by optimizing the beam modulation in the treatment planning system (TPS).

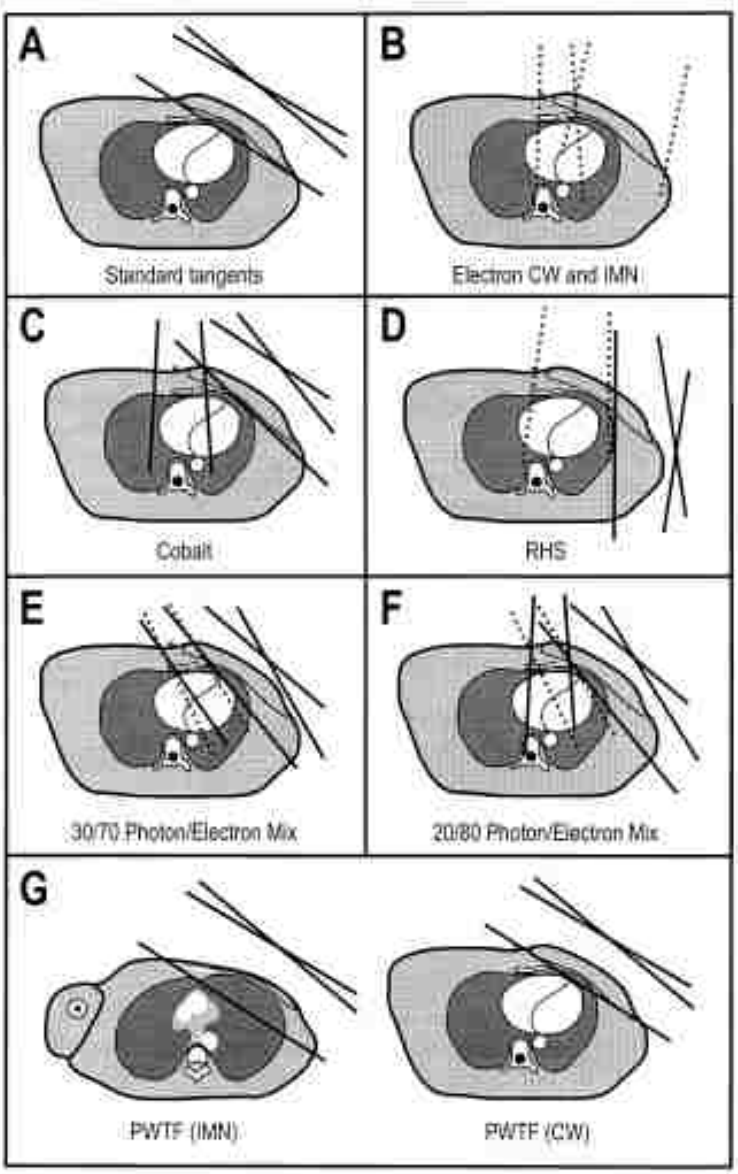

Figure 1-2: Traditional treatment techniques [15]

Their results showed that the IMRT technique matched the excellent heart sparing of the PWTF technique while also achieving substantially more uniform doses to the chest wall and internal mammary nodes due to the reduction in field junction problems. The IMRT plan also achieved slightly lower dose to the ipsilateral lung, but slightly higher volumes of low doses to

the contralateral lung and contralateral breast.

B. TomoTherapy

1) Hi-Art Treatment System

The TomoTherapy Hi-Art treatment system is a specialized modality for the delivery of intensity modulated radiation therapy treatments. It was designed and developed by Mackie et al. [16] and treatment of patients began in 2002. The name TomoTherapy means "slice" therapy and it is on this basis that TomoTherapy works. The gantry rotates around the patient while the patient simultaneously moves through the bore resulting in a helical delivery pattern (Figure 1-3).

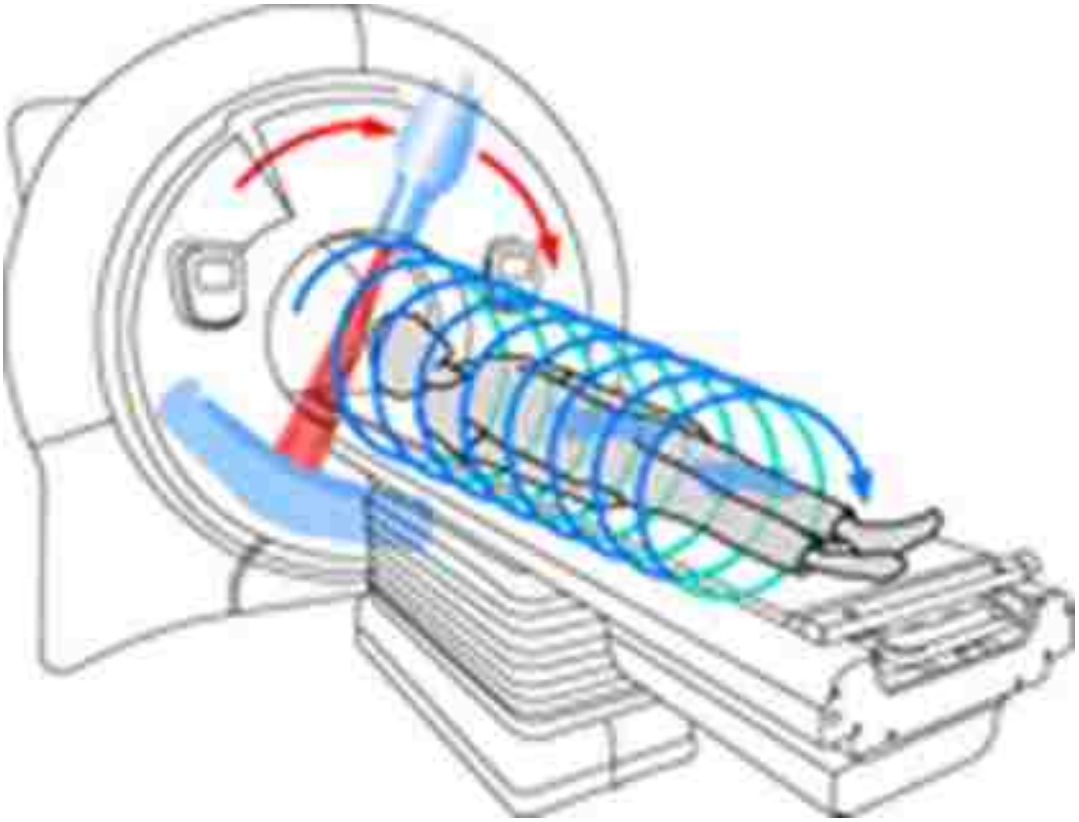

Figure 1-3: TomoTherapy helical delivery pattern

TomoTherapy greatly reduces the risk of high or low dose deposition in areas of field junction or overlap because these areas are blurred by the helical delivery. An assessment of earlier sequential units showed that patient positioning errors even as small as 1 mm could cause dose errors as high as 10-20% in the abutment regions [17].

TomoTherapy combines a linear accelerator and computed tomography (CT) gantry in the same machine. The slip-ring technology of the CT system is used to transmit power and data while allowing for 360° rotations of the linear accelerator. This allows for continuous radiation delivery as the linear accelerator rotates around the patient, as well as the ability to treat large volumes with multiple, continuous gantry rotations. TomoTherapy also has the ability to provide pretreatment megavoltage CT (MVCT) images which can be used as image guidance to properly position the patient prior to treatment delivery.

The mechanical design of TomoTherapy consists of a 6 MV accelerator, tungsten jaws, a 64-leaf binary multi-leaf collimator (MLC), and an exit detector array opposite the treatment head (Figure 1-4). The jaws are adjustable to create a fan beam with thickness from 0.5 cm to 5 cm in the inferior/superior direction as the patient is on the couch, but they are fixed during delivery. Intensity modulation as well as field width is achieved through the binary MLC. Thus, the MLC can create a fan beam field up to 40 cm wide. Each leaf projects to a width of 0.625 cm at the center of the bore with radius 85 cm.

The exit detectors on the TomoTherapy treatment machine consist of a 1D array of 738 xenon gas ion chambers (the central 640 are used to detect exit radiation) aligned opposite the 6 MV linear accelerator. For imaging, the beam energy is reduced to 3.5 MV and the same ion chamber array is used. A lower energy beam is better for imaging due to a number of reasons which have been discussed by Ruchala et al. [18].

Prior to treatment, a computed tomography image is taken with the patient in the treatment position. Since this image is acquired with a megavoltage energy beam (3.5 MV) it is referred to as MVCT. The MVCT image is registered with the planning kVCT (kilovoltage computed tomography) image to determine the required shifts to correctly position the patient relative to the treatment beam. This technique is known as image guided radiation therapy (IGRT).

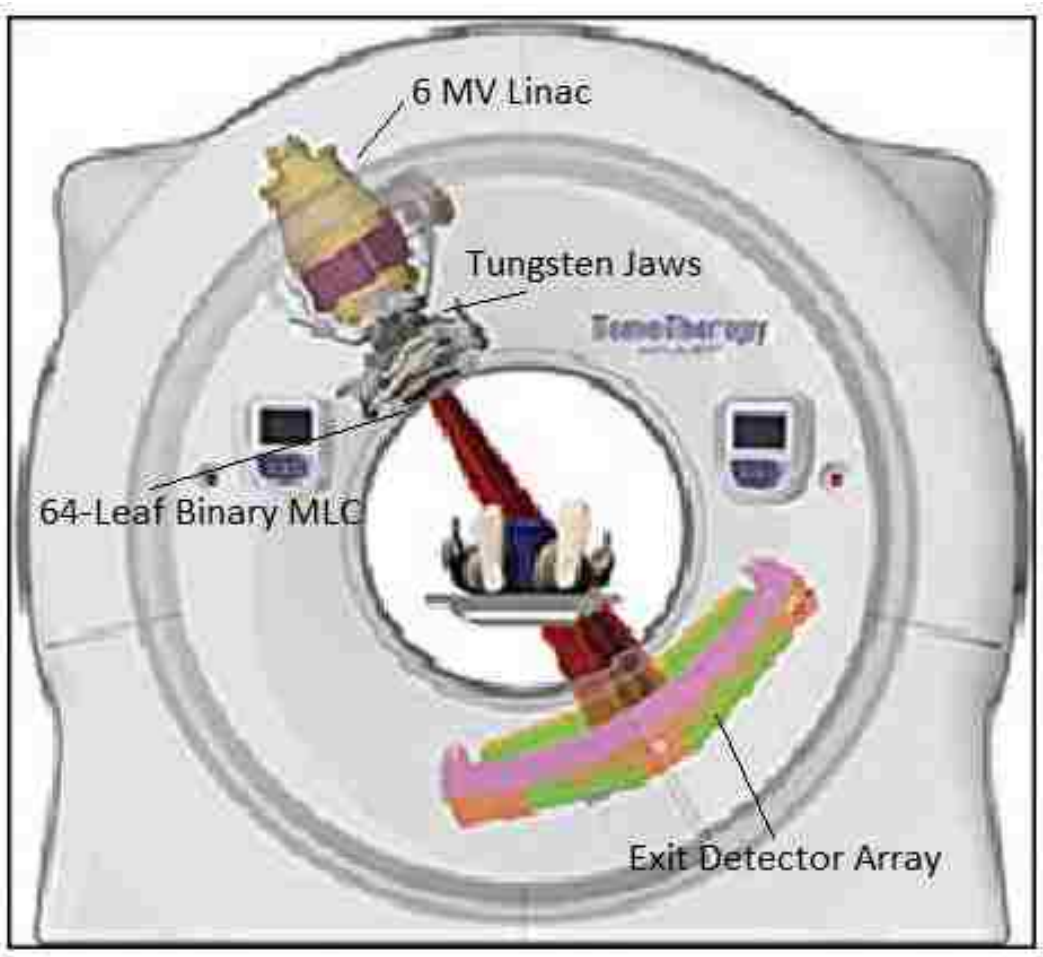

Figure 1-4: TomoTherapy mechanical configuration

2) Superficial Treatments

One area of potential concern with TomoTherapy is its use in the treatment of superficial targets. A study at Mary Bird Perkins Cancer Center (MBPCC) by Cheek et al. [19] reported that the TomoTherapy Hi·Art II treatment planning system (v. 2.2.4) overestimated dose at depths less than 1 cm by as much as 9.5% for measurements made on a cylindrical polystyrene phantom.

Three treatment plans were created for the cylindrical phantom with a 2 cm, 4 cm, or 6 cm PTV contoured on the surface of the phantom. An avoidance contour was created in each of the plans generating a resemblance to a patient being treated for PMRT. Radiochromic film was placed in the center of the phantom to measure the dose distribution delivered during the treatment. The measured dose distribution was compared to an extracted planar dose distribution from the TomoTherapy treatment planning system calculations. Differences in the two dose distributions can be seen in Figure 1-5, and they are most severe at depths less than 1 cm for each of the three cases studied.

These differences were believed to be due to limitations of the TomoTherapy dose calculation algorithm, such as the shape of the dose kernel for oblique incidence near the surface and the modeling of the rotational delivery as 51 equally-spaced static beams. Based on these results, MBPCC adopted the use of 1 cm of thermoplastic bolus material in treating all PMRT cases with TomoTherapy. The use of this bolus material placed the skin surface at a depth where the TomoTherapy dose calculations were within 5% of measurement.

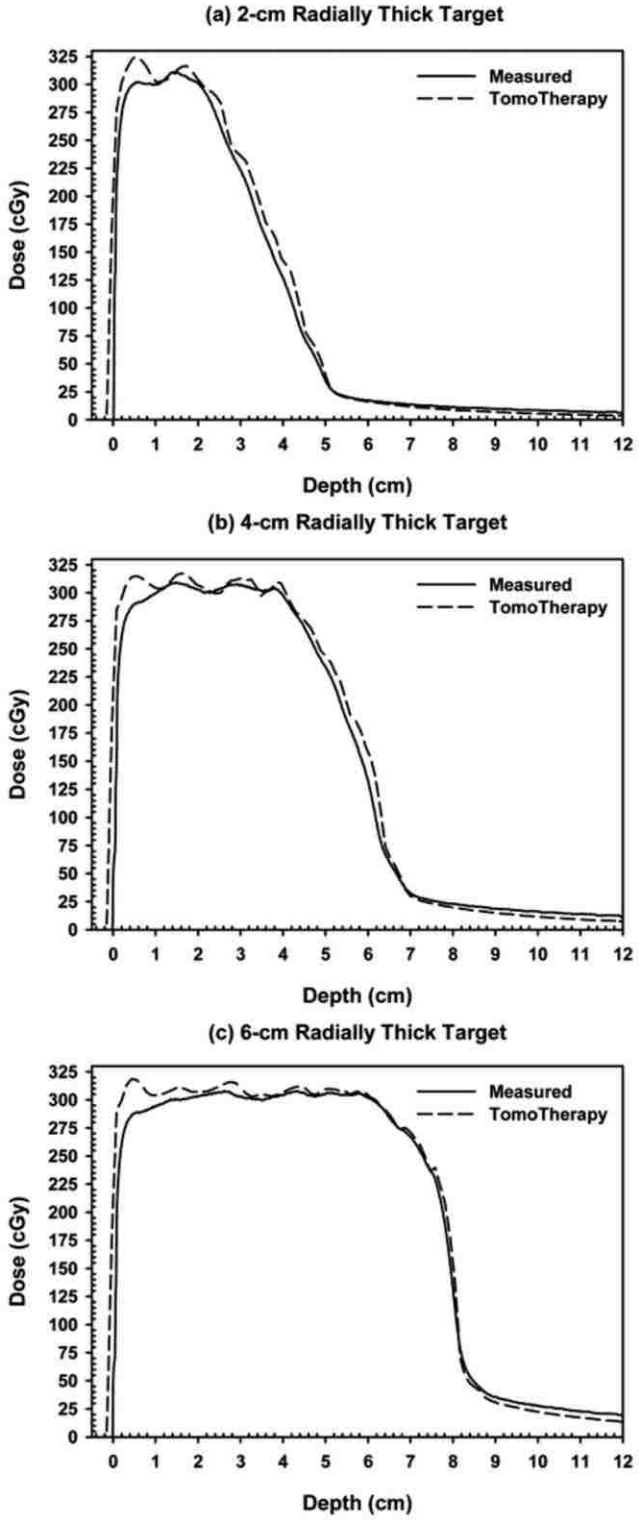

Figure 1-5: Comparison of TomoTherapy calculations with measured mid-arc depth-dose curves for (a) 2, (b) 4, and (c) 6cm radially thick PTV's [19]

3) PMRT

(a) Feasibility

As was shown by Krueger et al. [13], the use of IMRT improved the dose distributions for patients undergoing PMRT treatments. Arcing IMRT is the next step in the progression from fixed beam IMRT, and it allows for yet one more degree of freedom with gantry motion during IMRT delivery as well as completely avoiding field junction problems [20]. TomoTherapy is one such approach to this technique, and it has been shown by Ashenafi et al. [21] to be a feasible treatment method for PMRT.

In a planning study comparison of conventional mixed-beam treatment plans with TomoTherapy, the TomoTherapy plans showed significant improvement in dose uniformity to the PTV and an increased tumor control probability. Figure 1-6 shows typical dose distributions for PMRT treated with a traditional mixed beam plan compared to a TomoTherapy plan. The TomoTherapy plan avoids hot and cold spots encountered in the field abutment regions of the mixed beam plan. However, the TomoTherapy plans showed an increased volume of low dose to the lungs, contralateral breast, and non-specified normal tissue which could be of concern, particularly in younger patients who may have an increased but uncertain risk of developing a secondary cancer.

Based on TomoTherapy's ability to avoid field abutment complexities and the significant improvement in dose uniformity seen in the PTV, Mary Bird Perkins Cancer Center has since been using TomoTherapy as treatment of choice for PMRT.

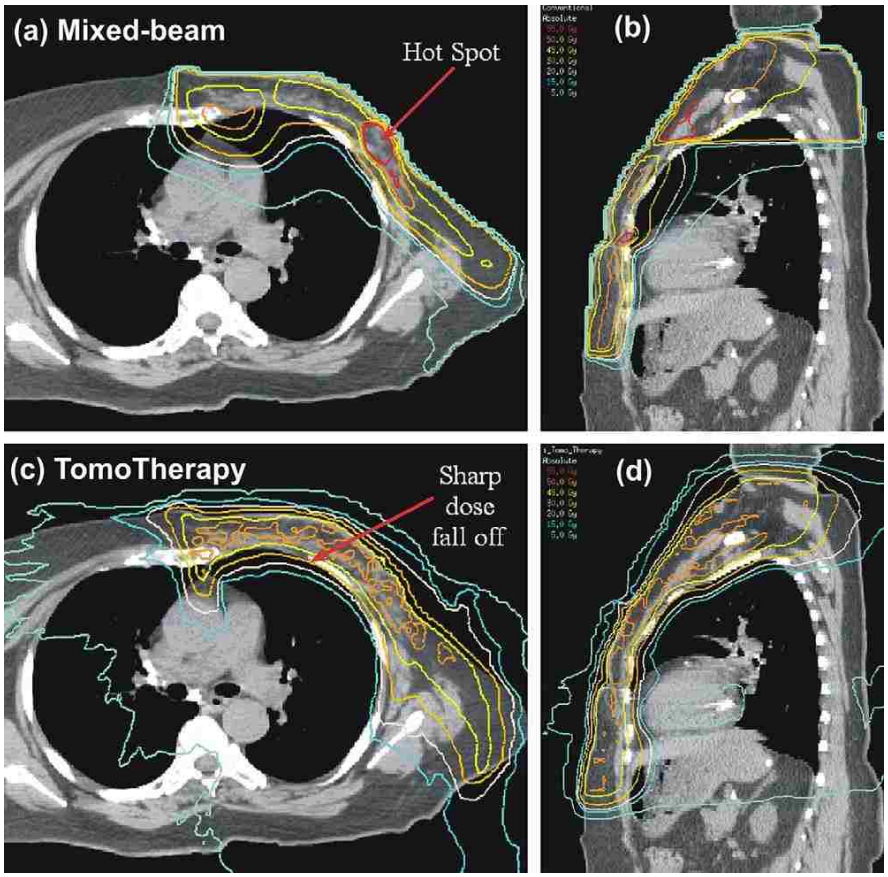

Figure 1-6: Transverse and sagittal views of dose distributions for (a,b) conventional mixed-beam plan and (c,d) TomoTherapy plan taken through IMN region [21]

(b) In-Vivo Dose Verification

Since the use of TomoTherapy for PMRT was a new treatment method at MBPCC, radiation oncologists ordered in-vivo dosimetry to assess the dose delivered to the skin surface of the chest wall. To verify the accuracy of calculated skin doses, Ito et al. performed a total of 298 in-vivo chest wall TLD measurements on 5 patients for comparison with calculated doses from the TomoTherapy treatment planning system [22]. All measurements in the Ito study were placed around the mastectomy scar, a relatively small region of the treated chest wall surface. To supplement this data, an additional 122 measurements were made on 5 patients at skin surface points throughout the treated chest wall region. In general, the agreement between measured and

calculated doses was good: the 420 measurements showed an average deviation of the TLD doses of -2.1 ± 0.2 % compared to the calculated doses. However, the standard deviation of the data was large at 4.5%, with a range of -18.4% to 12.6%. This indicates that while the total dose delivered to each TLD location was within clinical acceptability, there exists the potential for large individual (i.e., treatment fraction) fluctuation in delivered dose during PMRT. Figure 1-7 is a histogram showing the number of each deviation in 1% bin sizes, and the dashed line is a Gaussian with a mean of -2.1% and standard deviation of 4.5% as calculated from the measured data.

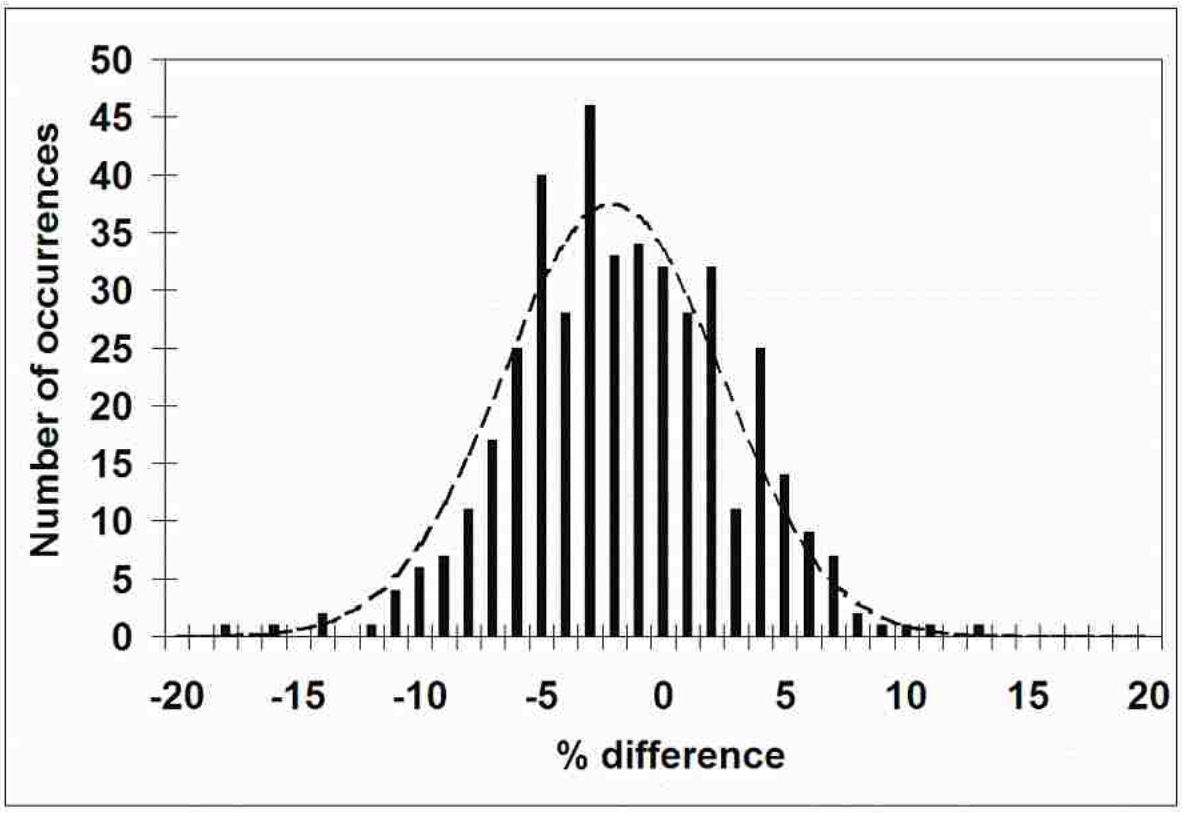

Figure 1-7: Difference between patient TLD doses and TPS calculated doses collected in 1% bin sizes with a dashed Gaussian fit

The causes of the measured deviations are not clear, but may include intrafraction motion including respiratory motion, air cavities between the bolus and patient skin surface, changes in patient anatomy throughout the course of treatment, errors in the TomoTherapy treatment planning system (TPS) calculations, variations in TomoTherapy delivery output, MLC leaf open time errors, and uncertainties and/or errors in the comparison measurements.

To investigate these possible errors further, it is desirable to have a method to evaluate the delivered dose to points throughout the chest wall surface without the need for regular in-vivo dose measurements.

C. Delivery Verification and Dose Reconstruction

1) Overview

To address the need for this type of analysis without in-vivo dosimetry, TomoTherapy has developed its delivery verification planned adaptive (DVPA) software. The DVPA software uses the exit detectors on the TomoTherapy treatment machine to collect data on the treatment delivery and verify the delivered energy fluence. It then uses the collected data and the pretreatment MVCT image to reconstruct dose delivered to the patient during the treatment fraction. If clinical targets are found to not be receiving the proper radiation dose throughout the course of treatment, the patient's plan can be modified to account for the changes. This is known as adaptive radiation therapy.

In order to perform dose reconstruction, two things are needed by the DVPA software – an image dataset and energy fluence information. The software computes dose using a convolution/superposition algorithm, which is also used by the TomoTherapy TPS. DVPA allows for the use of either the original planning kVCT image set or the pretreatment MVCT image set. It is also possible to use either the planned energy fluence from the TPS or delivered

energy fluence as calculated from the exit detector data collected during the treatment. It is expected for the planned and delivered energy fluences to be equal, but small deviations may occur due to mechanical issues with TomoTherapy such as output drift or inaccurate leaf open times. For instance, TomoTherapy's beam output is allowed to vary by up to 5% over 5 seconds or 50% for 1 second before the machine is interlocked and treatment stopped. Also, the machine will interlock if there are 4 instances where the MLC leaf open time differs by more than 32 ms from the planned leaf open time [23].

Kapatoes et al. [24-26] describe a method for determining the energy fluence used in delivery verification (DV) and dose reconstruction (DR) using the exit detector signal. The signal (s) in any detector element (i) can be represented as a weighted (d) sum of the energy fluence (ψ) emitted from each MLC leaf (j) as shown in the following equation.

$$s_i = \sum_j d_{ij}\,\psi_j$$

When expressed in vector-matrix notation the equation can be written as

$$s = D\psi$$

where s is the vector of exit detector signal, ψ is the vector of energy fluence, and D is the matrix of detector signal in the detector per unit of energy fluence from the MLC. Thus, D is a measured transfer matrix used to convert between detector signal and fluence. The energy fluence from a delivered treatment can be obtained by multiplying the inverse of the D matrix by the detector signal:

$$\psi = D^{-1}s$$

The method uses a linear model to relate detector signal and energy fluence so that energy fluence, leaf open times, and detector signal are all proportional to each other. TomoTherapy stores information relating machine state (e.g., fluence, leaf open time, and signal)

versus time for either measured data or the initial plan in the form of sinograms. The leaf-control sinograms show planned or computed leaf open times versus projection number for each treatment delivery. When measured data are used to compute the leaf open times this sinogram is called the DV sinogram.

The D matrix must be measured by opening each MLC leaf individually and recording the exit detector signal with the patient in the treatment position. There are obvious reasons why this is a poor method including the time it would take and the additional dose it would deliver. Exit signal from a radiotherapy beam is a function of the primary and scatter radiation received by the detector which can be expressed as a function of two parameters: the radiological path-length (RP) and the distance from patient to detector (DPD) respectively (Figure 1-8). For any given ray through the patient, RP is defined by

$$RP = \rho_1 L_1 + \rho_2 L_2 + \cdots + \rho_n L_n,$$

where ρ_i is the physical density of the material i through which the ray passes, and L_i is the length of the ray in that material.

By creating a measured database of detector profiles for several different values of RP and DPD, the D matrix can be reconstructed to relate signal to energy fluence by computing the values from the MVCT image and using them to access the database. The DVPA software uses this database method to create the DV sinogram and applies the beam output from the monitor chambers in the TomoTherapy treatment machine to obtain delivered energy fluence. The energy fluence is then applied to the MVCT image using the convolution/superposition algorithm. The following flowchart in Figure 1-9 illustrates how this method is used for the DV and DR processes.

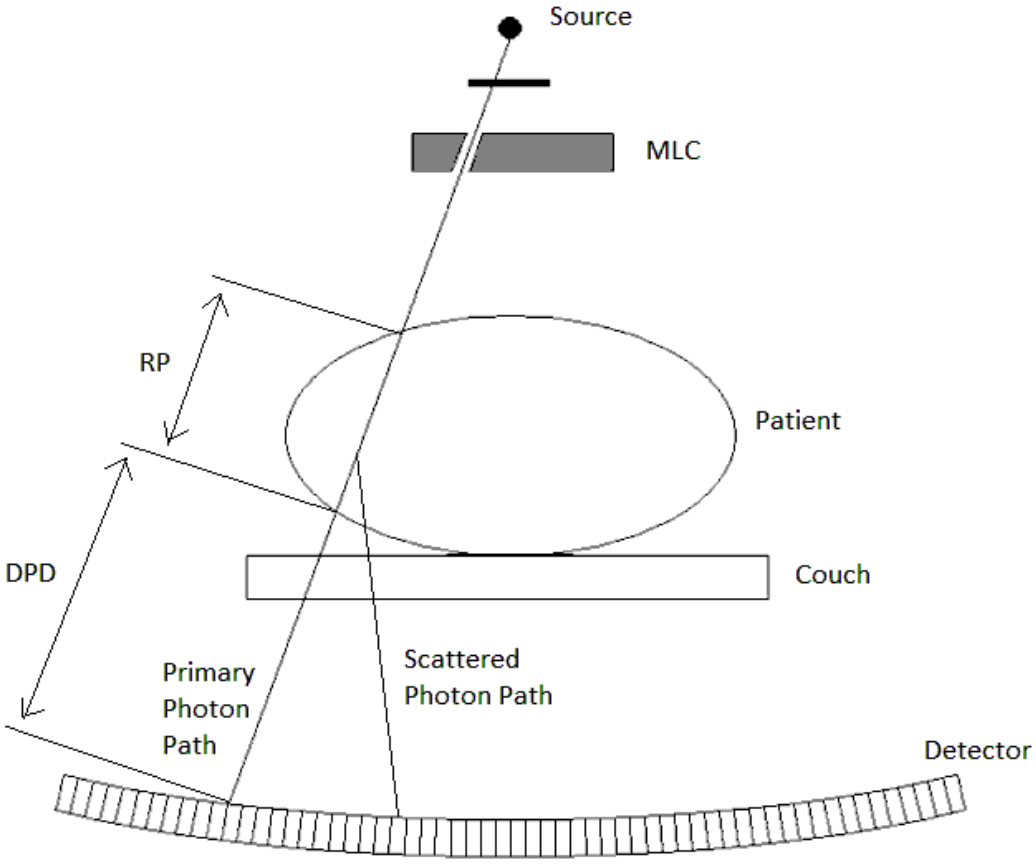

Figure 1-8: TomoTherapy exit detector diagram showing RP and DPD relationships

2) Accuracy

A previous study by Hesston et al. showed that DV and DR using TomoTherapy DVPA software is accurate within 2% for a point dose measurement made with ion chamber and has a passing gamma analysis value of less than 1 for 90% of the film region of interest [27]. However, several aspects of the study by Hesston et al. differed from this current study. The treatment sites chosen were head & neck, prostate, and lung, and thus did not have the complication of being at the patient's surface. Also, the DVPA software did not use the database method for computing the DV sinogram. Instead, the threshold method was used, whereby the

full width-half max (FWHM) of the pulse-by-pulse exit detector signal was used to compute the leaf opening times which were then adjusted based on output variations.

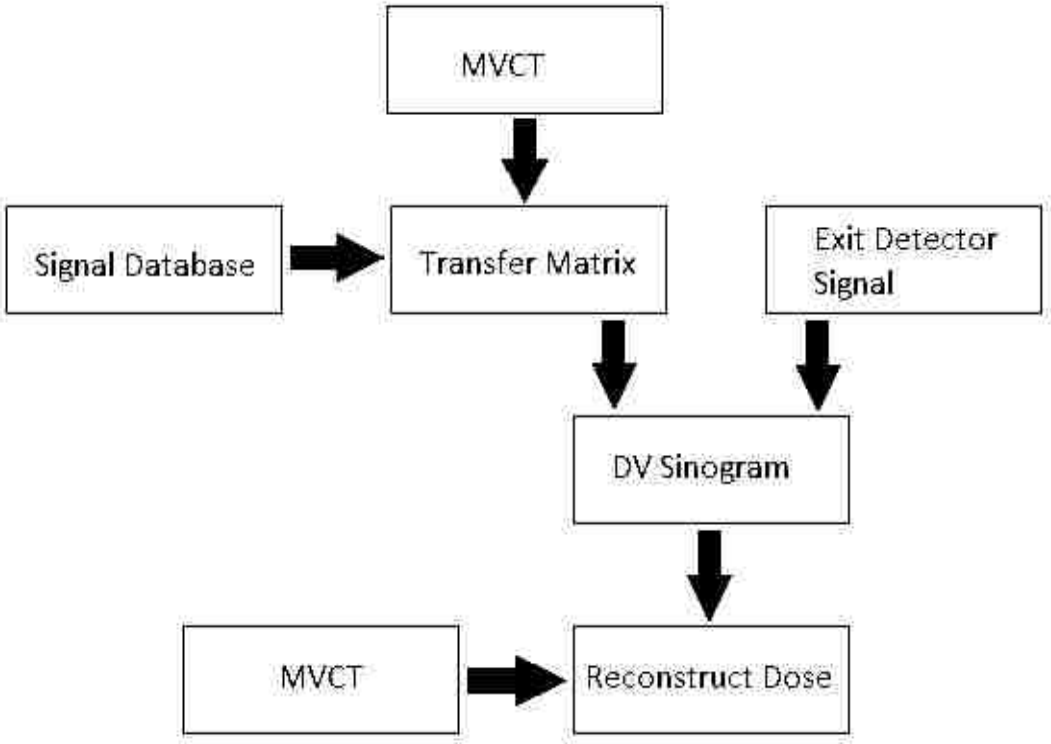

Figure 1-9: Flowchart illustrating delivery verification and dose reconstruction

The threshold method measures exit detector dosimetry data for each pulse of the linear accelerator, which operates at a rate of 300 pulses per second. A single open MLC leaf irradiates approximately 7 elements of the exit detector array. The central five elements (of these 7) are used to compute leaf open time by measuring the average FWHM of the signal profile. Measured output data from the monitor chambers is then compared to planned output, and the leaf open times are scaled by this ratio to determine effective leaf open times. The DV sinogram

can be calculated after all of the effective leaf open times have been determined. Delivered energy fluence is then derived from the DV sinogram and planned beam output [27].

An ion chamber was also used in the dose comparisons in this study, as opposed to TLDs which have a relatively higher level of uncertainty in their measurement of delivered dose as compared to ion chambers. One more difference is that the previous study computed the DR on the planning kVCT as opposed to the MVCT images representing actual patient position at the time of treatment delivery.

Something that should be noted about the use of the database method for DV and DR is that calculation of RP on voxels on the surface will have partial volume effects as an inherent limitation of the method. This may have problematic effects for treatments involving superficial targets. Also, intrafraction motion may cause rapid and periodic changes in RP which may also impact DV and DR with the database method [24].

The database technique has a major benefit over the threshold technique, in that it can be used for retrospective data analysis. The threshold technique uses pulse-by-pulse exit detector data which is only stored for the most recently delivered treatment. In order to use the data for DV and DR, it must be downloaded immediately after a patient's treatment has been delivered. The database technique, on the other hand, uses exit detector data measured on a projection-by-projection basis. This data is typically compressed by a factor of ~100 compared to the pulse-by-pulse data. Thus, it is saved in the patient archive files and can be used in the future for a retrospective analysis of the patient's dosimetry data.

II. Hypothesis and Specific Aims

The hypothesis of this study is that corresponding TomoTherapy DVPA calculated doses and patient (or phantom) in-vivo TLD doses will agree within 5% for 95% of data points and

10% for all data points.

The following specific aims will be performed to complete the research project:

Aim 1: Use TomoTherapy's DVPA software to calculate the point doses at the estimated coordinates of the patient TLD locations measured by Ito et al. and compare them to the measured clinical TLD doses.

Aim 2: Image RANDO phantom (The Phantom Laboratory, Salem, New York, USA) and plan a typical chest wall PMRT treatment with TomoTherapy TPS. Deliver TomoTherapy treatment to RANDO phantom with TLD's in place on the chest surface of the phantom.

Aim 3: Read out TLD doses from the RANDO phantom and compare them to DVPA reconstructed doses and treatment planning system doses.

Chapter 2. Methods and Materials

I. Aim 1

The purpose of Aim 1 was to use TomoTherapy's DVPA software to calculate point doses at the estimated locations of the patient TLD's from the work of Ito et al. and compare the calculated point doses to Ito's measured TLD doses.

A. Patient Data Restoration

A previous in-vivo TLD study on TomoTherapy PMRT was performed by Ito et al. [22]. They compared the doses delivered to TLD's placed on the skin surface surrounding the mastectomy scar of five patients undergoing PMRT with TomoTherapy to the expected doses calculated in the original treatment plans. Using the TLD dose data that was measured, the archived patient exit detector data, and MVCT image data from the treatments; the calculated delivered dose can be reconstructed for comparison with the measured doses.

A total of five patients were used in the collection of data by Ito et al. Each patient had had several radiopaque markers placed on the skin surface surrounding the mastectomy scar prior to CT simulation. Four of these locations were chosen for TLD placement on each of the patients (Figure 2-1 through Figure 2-5). Patient TLD doses were measured for 15 of the 25 treatment fractions. Measurements were acquired for each treatment during the first week and alternating fractions throughout the remaining course of treatment.

When TomoTherapy patients complete their treatments at MBPCC, all the information regarding their plans and treatment data – including all exit detector data, monitor chamber data, and MVCT images that were collected during successful TomoTherapy treatments – is stored on digital media and placed in the patient archive. Archived data for each patient in the Ito study

were located and restored on the TomoTherapy DVPA analysis computer using the DV Operator Station. The patients were identified as A – E to correspond to the patient identifiers used in the Ito study. Archived patient data were also restored to the Planned Adaptive Software (version 3.1.2) to overlay and compare different image data sets when locating the TLD positions.

Figure 2-1: Photo and 3D skin rendering showing locations of TLD placement for Patient A

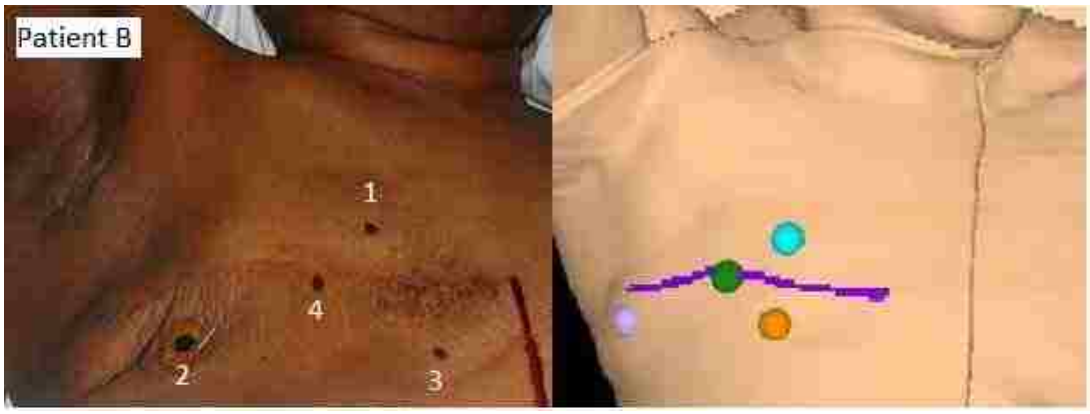

Figure 2-2: Photo and 3D skin rendering showing locations of TLD placement for Patient B

Figure 2-3: Photo and 3D skin rendering showing locations of TLD placement for Patient C

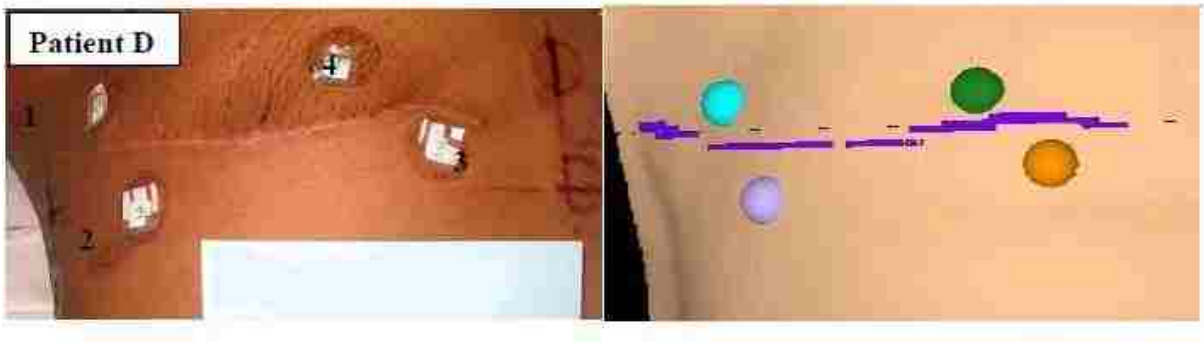

Figure 2-4: Photo and 3D skin rendering showing locations of TLD placement for Patient D

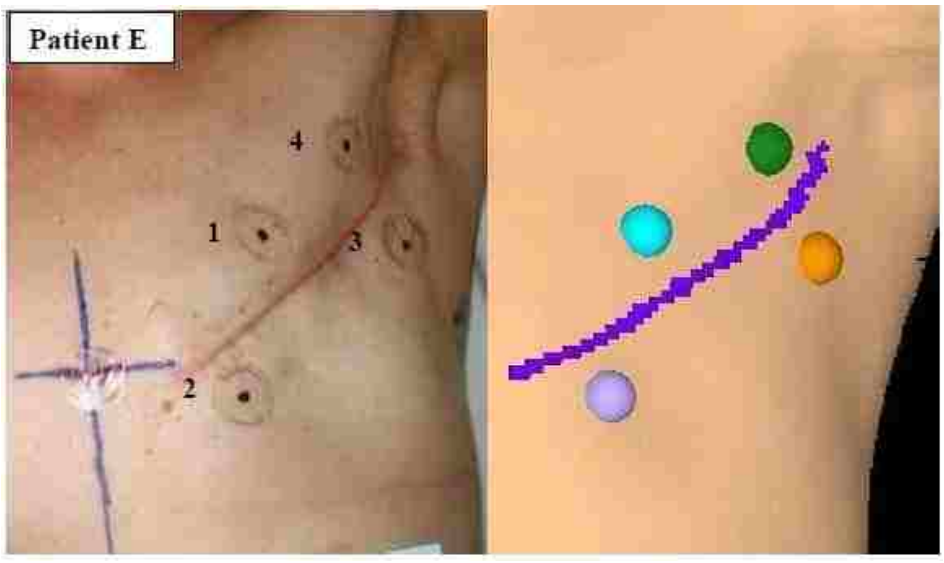

Figure 2-5: Photo and 3D skin rendering showing locations of TLD placement for Patient E

B. Delivery Verification and Dose Reconstruction

Using the MVCT images and exit detector data from each fraction that in which TLD data was acquired, delivery verification sinograms were computed for dose reconstruction on the MVCT images.

One 360° rotation of a TomoTherapy delivery is segmented into 51 projections of approximately 7° per projection. After each treatment delivery fraction, the projection-by-projection exit detector delivery data is automatically stored in the patient archive. Since the data is stored as a cumulative projection-by-projection signal as opposed the raw detector data which is acquired pulse-by-pulse, the data is compressed by a factor proportional to the number of pulses per projection which is typically on the order of 100 [24]. This factor reduces both the storage space as well as computational time requirements for implementing the transfer matrix approach to delivery verification (DV) and dose reconstruction (DR).

To measure the true transfer matrix, exit detector data must be acquired with the patient in the treatment position on the couch. By using a measured database to reconstruct the transfer matrix, the time and extra dose to the patient it would take to do this is eliminated.

The database used in the delivery verification software was measured by TomoTherapy, Inc. It was created by obtaining detector data for several different thicknesses of solid water at varying distances from the detector. Solid water is a rigid plastic material that is manufactured to have similar radiological properties as that of liquid water. Some of these properties include physical density, electron density, and effective atomic number. The values for which these measurements were obtained to create a 3x12 database matrix are as follows:

RP = 0, 1, 2, 3, 5, 10, 15, 20, 25, 30, 35, 40 cm

DPD = 76, 70, 60 cm

When beamlet tracing measurements are taken from the MVCT images (as described in section 1-I-C-1) interpolation is used to obtain the values which are to be used when reconstructing the transfer matrix.

Figure 2-6 shows the options that were selected for DV and DR for each patient's treatment fraction in the DVPA software. For all patients, the registered MVCT images were used to take RP and DPD measurements for database access and DV sinogram reconstruction as well as the image set to reconstruct delivered dose.

MVCT images acquired by TomoTherapy only have a 40 cm field of view (FOV) as opposed to the FOV of the CT planning (reference) image which is usually larger (e.g., 50 cm FOV). The DVPA software allows the user to replace this missing image information either by air or by data from the reference CT. For this work, missing MVCT data would not lead to any errors in DV and DR because they were on the contralateral side of the patient because the patient's treatment area is moved towards the center of the CT causing missing data on the contralateral side. Each patient also had "avoid" ROI's placed in the "missing tissue" areas so no treatment beamlets were allowed to enter the patient through this region.

After the DV sinogram was computed for a patient, it was viewed alongside the planned sinogram to determine the differences in specific leaf open times that exist and where the differences occur in the treatment. Figure 2-7 shows a typical DV sinogram which was calculated from one of the patients used in this study. The figure is a partial view of the planned sinogram, reconstructed DV sinogram, and the difference between the two.

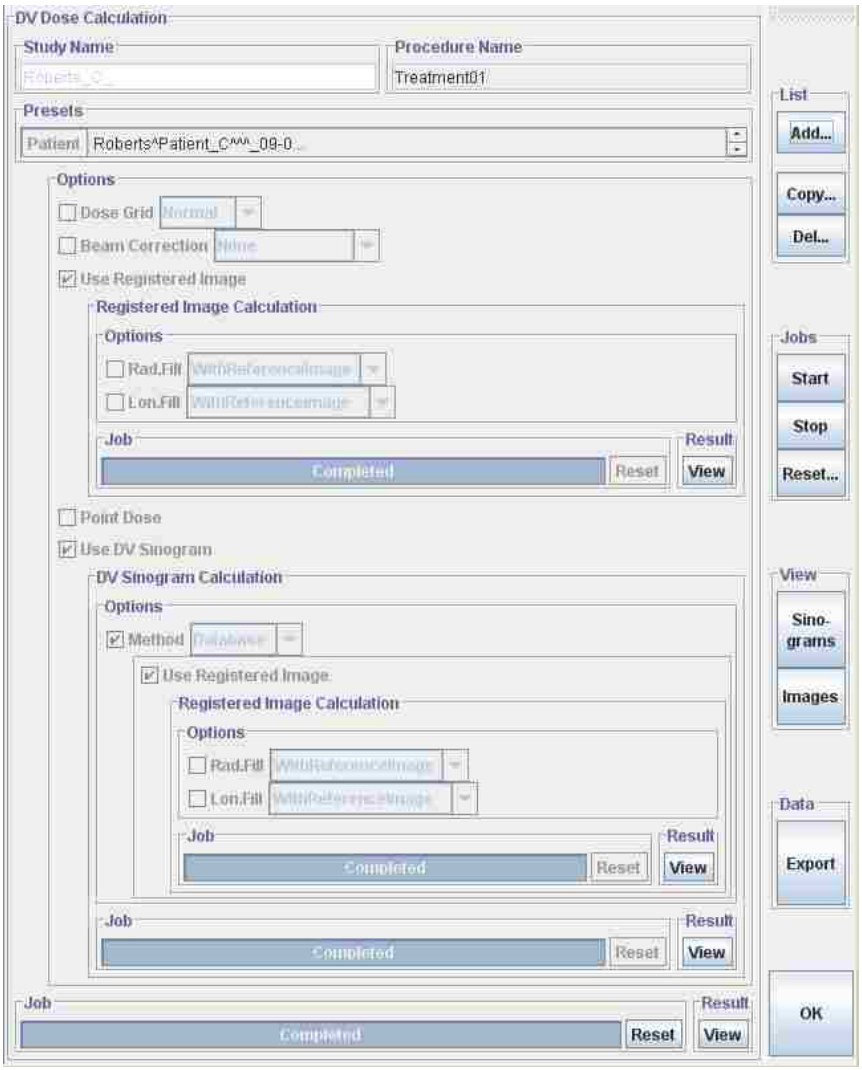

Figure 2-6: DVPA options used for DV and DR for each patient

The horizontal axis on the sinograms represents the MLC leaf number from 1-64 and the vertical axis represents the projection number of the treatment delivery. Every point in the sinogram graph represents the time that a specific leaf was open during a certain projection of the patient's treatment delivery, where time is represented by a color scale with black being closed, blue having relatively short open times, red having longer open times, and green being in the middle. In figure 2-7, the cursor is set at the same position in all three sinogram images so the leaf open time for the planned and reconstructed sinogram and their difference can be seen for

leaf 3 at projection 607.

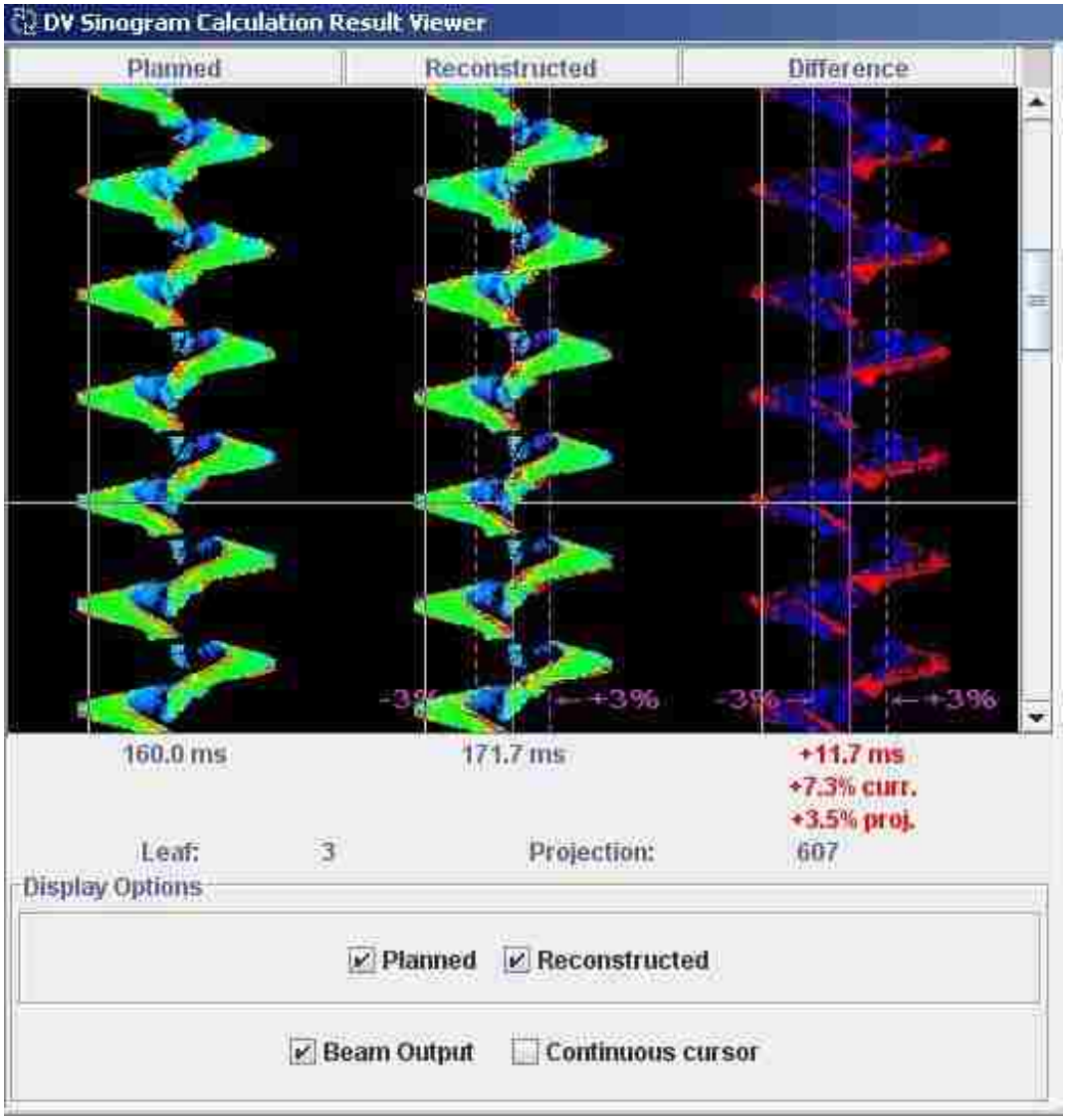

Figure 2-7: Sample comparison of the planned and reconstructed DV sinograms

C. Point Dose Extraction

Since the TLD packets are small and designed to be radiographically tissue equivalent, the position of the TLD's cannot be seen in the MVCT images. In order to determine the point doses from the dose reconstruction, the MVCT images from each of the daily patient fractions

were compared to the original planning kVCT images as well as photographs of the TLD's placed on the patient surface to determine TLD locations in the MVCT image. The kVCT images were acquired with radiopaque markers on the patient surface and four of the marker positions were selected for TLD placement for in-vivo measurements. At the time of treatment the kVCT and MVCT images were registered, putting them on the same coordinate system. Thus, by comparing coordinates in the corresponding slices in the registered kVCT and MVCT image sets along with the photographs of TLD position acquired at the time of treatment, the position of the TLD's can be approximated on the MVCT images (Figure 2-8 and Figure 2-9).

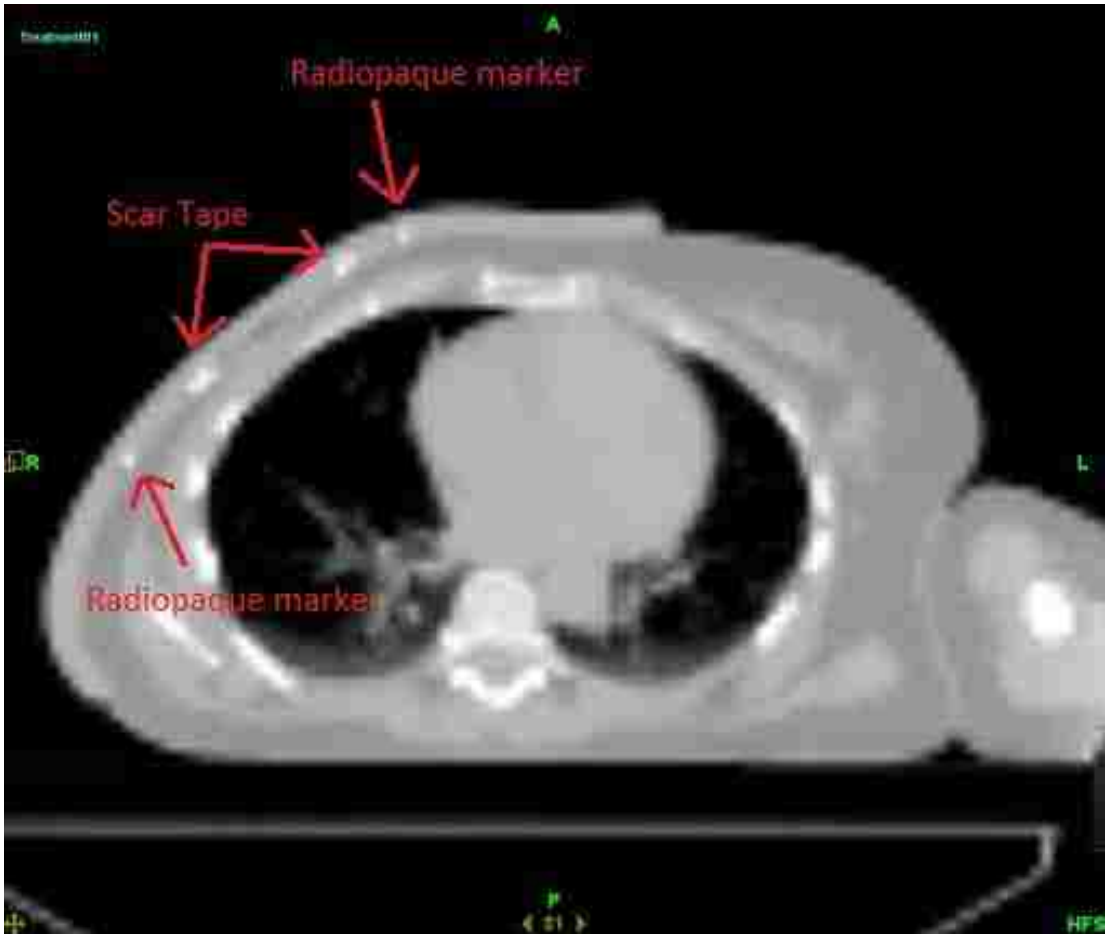

Figure 2-8: kVCT image showing positions of various radiopaque markers

The coordinates of the TLD packet in the MVCT image were visually compared to the coordinates of the radiopaque markers in the kVCT image for each fraction and each TLD position was determined. If any of the estimated TLD locations in the MVCT images were determined to be somewhere other than the patient surface (e.g. inside the bolus, inside the patient, or in the air gap region), the location was shifted perpendicularly towards the surface of the patient.

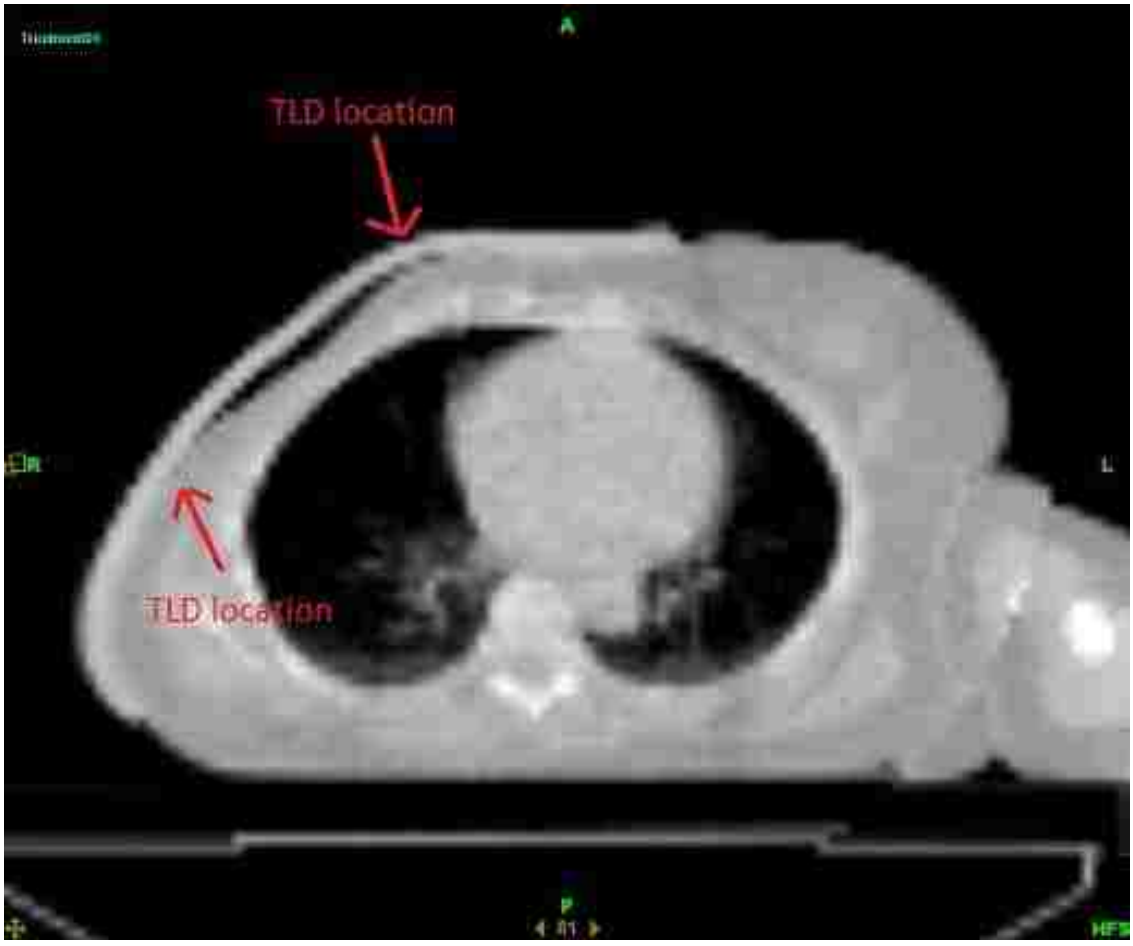

Figure 2-9: MVCT image showing the approximate locations of TLD packets based on comparison to the kVCT image

Since the TLD positions had to be estimated from coordinates on the kVCT images, DV

dose values were calculated for points at the estimated TLD location and points ±5 mm from the estimated TLD location in the lateral and superior-inferior directions. These five calculated doses were averaged to determine the mean reconstructed dose. This also allowed for the addition of an estimation of uncertainty in the reconstructed point doses from the DVPA software.

Mean point doses were calculated for each estimated TLD location using the dose reconstruction on the DVPA software for every fraction that the TLD's were measured. These point doses were compared to the TLD measured dose for each corresponding position and fraction, as well as the overall dose delivered to each location throughout the course of each patient's treatment. They were also compared to the dose that was expected from the original TomoTherapy plan.

D. Comparison of DVPA Doses and TLD Doses

Mean calculated DVPA doses were compared to both in-vivo TLD measured doses and the original treatment planning system calculations. This comparison provided information on how well the DVPA software agreed with measured data and how well the results compared with the planned doses approved by the radiation oncologist.

For each fraction the percent difference (Δ(%)) between the measured TLD dose and corresponding DVPA point doses were compared using the following equation:

$$\Delta(\%) = \frac{(T - D)}{T} * 100$$

Where T is the measured TLD dose and D is the reconstructed point dose from the DVPA software.

MATLAB (MathWorks, Natick, Massachusetts, USA) software code was written to perform linear regression analysis of the TLD measured and DVPA calculated doses for each

TLD location for each patient. Each patient had a total of 60 TLD measurements taken in 15 fractions of 4 TLD's each (except Patient E who only had 58). If for any reason a treatment was interrupted mid-fraction, the DVPA software was unable to compute dose reconstruction for that fraction. The numbers of valid TLD dose to DVPA dose measurements for comparison are shown in Table 2-1.

The data was also fitted with 95% confidence intervals (CI) and 95% prediction intervals (PI). A 95% CI gives the region where the linear regression should fall 95% of the time if the experiment is repeated. A 95% PI shows the region that 95% of the data points should fall if the experiment is repeated.

Table 2-1: Number of measurements for each patient

Patient	Valid Measurements
A	56
B	60
C	56
D	52
E	58
Total	282

II. Aim 2

The purpose of Aim 2 was to image the RANDO phantom and plan a typical chest wall PMRT treatment with TomoTherapy TPS; then to deliver the TomoTherapy treatment to the RANDO phantom with TLD's in place on the chest surface of the phantom.

A. CT Simulation

1) RANDO Phantom

For this study, the RANDO Man phantom was used in order to closely represent patient anatomical features during a typical PMRT treatment with TomoTherapy. The RANDO phantom was developed in order to provide an anthropomorphic phantom with uniformity of materials, size, and shape.

The phantom contains a natural human skeleton which is placed inside a molded soft tissue body contour. The soft tissue material of the RANDO phantom has a density of 0.985 g/cc (±1.25%) and an effective atomic number of 7.30 (±0.5%) which represents a composite of muscles, body fats, and fluids. The lung material has the same effective atomic number but a density of 0.3 g/cc (±1.25%). The phantom also contains air cavities representing the airways into the lungs. A total of 35 sections each 2.5 cm thick make up the phantom torso. The overall size of the phantom represents a person who is 5 feet 8 inches tall and weighs 162 pounds. (Figure 2-10)

2) CT Image Acquisition

As mentioned in section 1-I-B-2, all MBPCC PMRT patients are treated with a 1 cm thick thermoplastic bolus. To maintain consistency with clinical treatment procedures, a 1 cm thick sheet of thermoplastic bolus was molded to fit the chest of the RANDO phantom and allowed to cool for 24 hours before removal to ensure that it would not change shape as it cooled. The bolus was designed to cover the chest wall, supraclavicular lymph nodes, axial lymph nodes, and internal mammary lymph nodes. Whenever the phantom was not in use the bolus was kept in place on the chest of the phantom.

Figure 2-10: RANDO phantom used in this study

Radiopaque Clearline Scar Marker tape (The Suremark Company, Simi Valley, CA, USA) with a thickness of 2 mm was placed onto the chest of the phantom to represent the location and markings of a typical mastectomy scar. Eight XACT (Solstice Corporation,

Portland, ME, USA) 2.3 mm diameter radiopaque marker spheres were placed around the scar tape to mark the locations of TLD packets in the CT image. The spherical markers were placed approximately 4 cm from the radiopaque scar tape and approximately 4 cm from each other and they extended the entire length of the scar tape (Figure 2-11). They were placed on a piece of masking tape with their positions marked and numbered so that the corresponding TLD packet could be placed at the known location for treatment delivery.

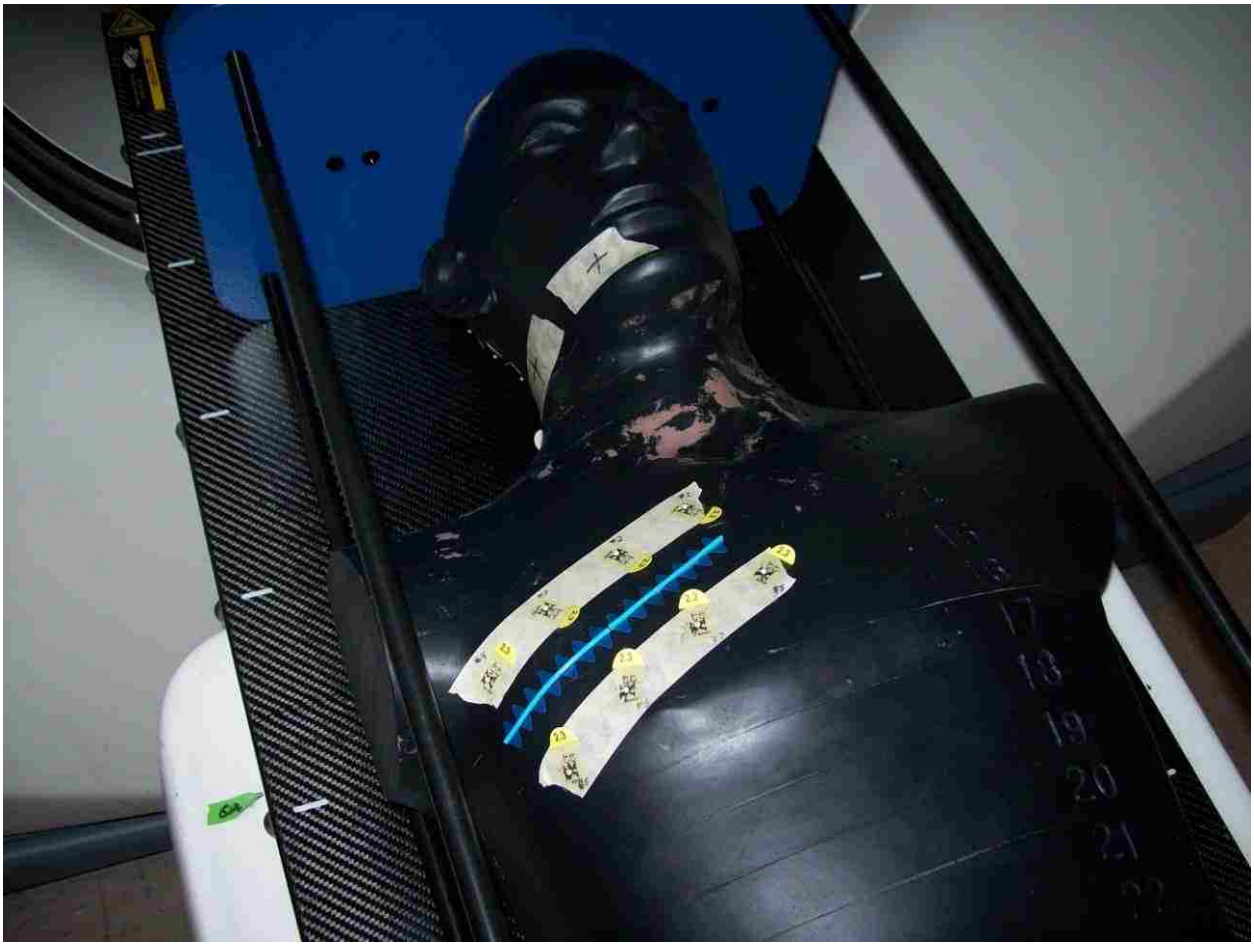

Figure 2-11: Picture of RANDO phantom with radiopaque scar tape and 2.3 mm spherical markers on chest surface

The RANDO phantom was scanned on a 16 slice GE LightSpeed RT (GE Healthcare, United Kingdom) CT scanner with the bolus and markers in place. The scan was acquired with the phantom in the headfirst-supine position with the following scanning parameters typical of a patient helical chest CT scan:

- 50 cm FOV
- 512 x 512 image matrix
- 2.5 mm longitudinal slice spacing
- 120 kVp
- 265 mA

B. TomoTherapy PMRT Treatment Planning

1) Transferring CT Image Dataset

After CT simulation, the image dataset was transferred to the TomoTherapy TPS as well as the Pinnacle^3 (Philips Healthcare, Andover, Massachusetts, USA) TPS. The 512 x 512 CT image dataset sent through the TomoTherapy DICOM was automatically down sampled to 256 x 256 axial pixel resolution because of memory limitations of the TomoTherapy TPS. All regions of interest (ROI) were contoured using the Pinnacle^3 TPS tools with the help of a certified medical dosimetrist (Figure 2-12). After all the contours were complete, the ROI dataset was exported from Pinnacle^3 to TomoTherapy TPS for treatment planning.

The PTV contour was designed to cover the chest wall as well as regions where the axillary, supraclavicular, and internal mammary nodes would be located in a typical patient. The lungs, heart, spinal cord, liver, and airway were contoured to serve as dose limiting organs at risk (OAR).

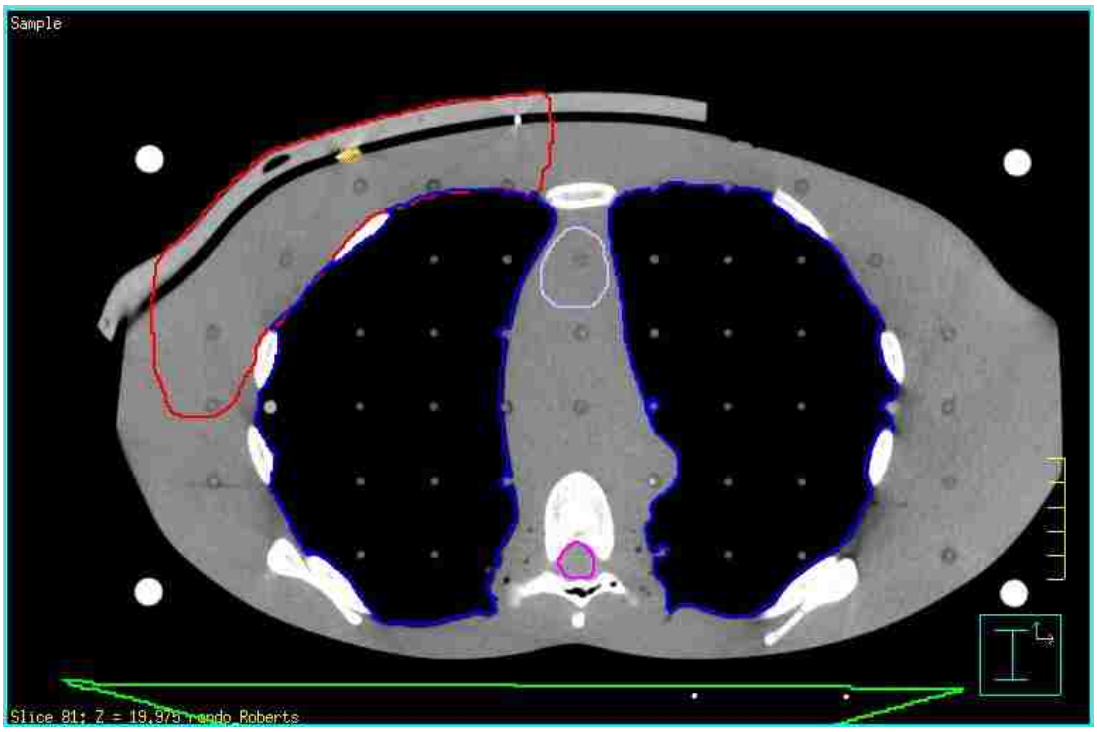

Figure 2-12: Pinnacle[3] image with ROI contours (Red - PTV, Blue - Lungs, Purple - Heart, Pink - Spinal Cord, Orange - Scar)

2) Treatment Planning

Treatment planning was done using TomoTherapy TPS version 4.0.2.4. The treatment plan was designed using MBPCC clinical TomoTherapy PMRT planning parameters. The plan had the following plan parameters:

- Prescription: 50 Gy in 25 fractions (2 Gy per fraction)
- Jaw Width: 5 cm
- Pitch: 0.287
- Modulation Factor: 3.0
- Dose Grid: Normal
- Optimization Mode: Beamlet

After the plan was finalized it was transferred to the TomoTherapy treatment delivery system.

C. Treatment Delivery

A total of three treatment fractions were delivered to the RANDO phantom. Before each fraction, an MVCT was acquired with the phantom in the treatment position. This was done to verify the setup location as well as provide the MVCT image dataset for dose reconstruction. The MVCT images were acquired without the radiopaque markers in place but with the bolus on the chest surface (Figure 2-13). Normal slice thickness (4 mm) was used and the range of slices was approximately 22 cm to cover the entire PTV with approximately 5 cm margins.

Figure 2-13: Image of RANDO with thermoplastic bolus on chest surface

After the MVCT image was acquired, numbered TLD packets were placed on the corresponding numbered locations previously marked for the spherical radiopaque marker positions. Figure 2-14 is a photograph of the RANDO chest surface with TLD packets in place and Figure 2-15 is a 3D rendering of the phantom showing the locations of the spherical radiopaque markers. The bolus was replaced and the TomoTherapy treatment was delivered as planned. The TLD packets were placed after the MVCT acquisition so they did not receive any dose from the MVCT scan.

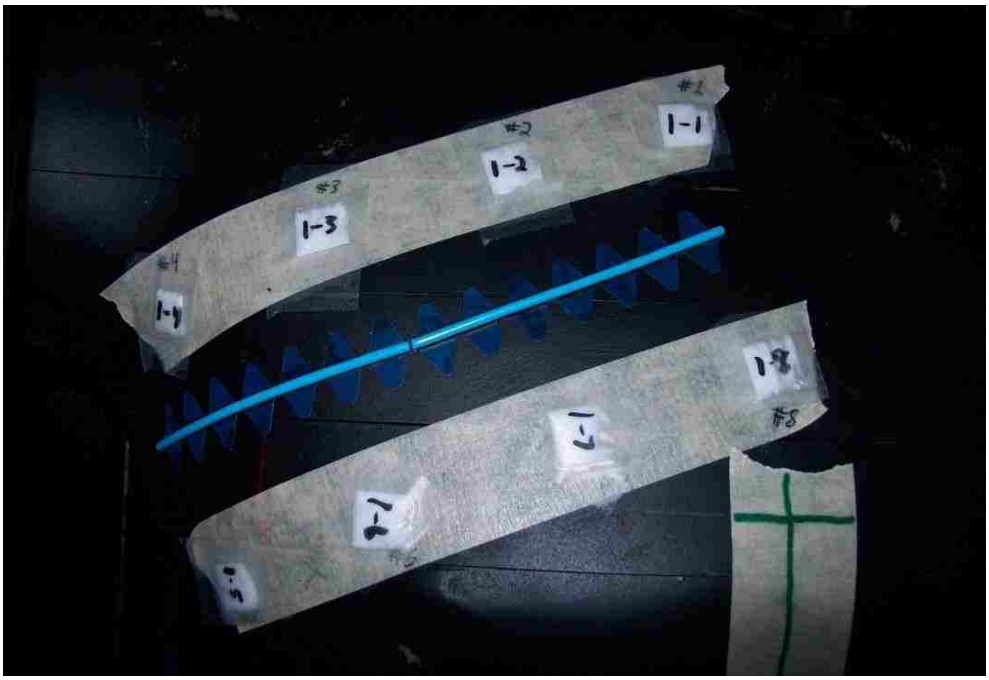

Figure 2-14: TLD packets in place on RANDO phantom

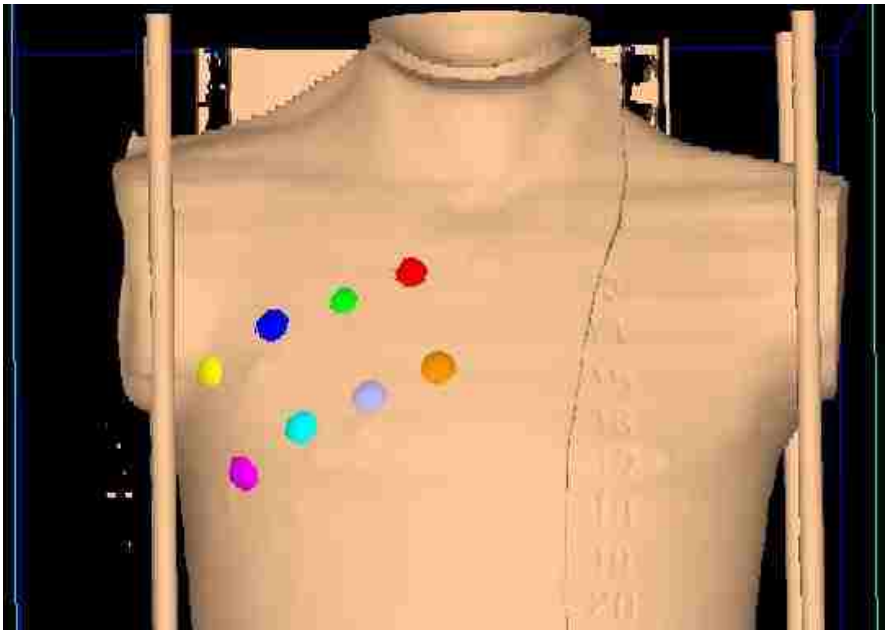

Figure 2-15: 3D rendering of radiopaque marker locations. Marker structures are for display purposes only and are not to scale.

III. Aim 3

The purpose of Aim 3 was to compare measured TLD doses to the original treatment planning system calculations and DVPA reconstructed doses for treatment delivery to the RANDO phantom.

A. TLD Measurement Procedures

1) Packet Preparation

Several TLD packets were prepared at the same time and from the same batch of LiF-100 TLD powder. Enough packets were prepared for the phantom delivery, calibration, and background readings. The packets were approximately 1 x 1 x 0.2 cm^3 and contained approximately 45 mg of powder in each. All TLD packets were kept together until the time of delivery, and again until time of readout so that any background radiation collected by the TLD would be the same for each packet and so all the TLD maintained the same thermal history.

2) Treatment Delivery

A total of 24 TLD packets were used in three delivery fractions of eight TLD's each. As mentioned in section 2-II-C they were numbered and placed on the corresponding location of the RANDO phantom chest surface before being covered with 1 cm of thermoplastic bolus and having the TomoTherapy treatment delivered. The packets were not in place during the pretreatment MVCT image. The first and second treatment deliveries were spaced two weeks apart, and the third treatment delivery was one week after the second.

3) Calibration

Calibration TLD packets were irradiated to known doses (150 cGy, 200 cGy, 250 cGy) surrounding the expected treatment dose of 200 cGy. The doses were delivered on a BrainLAB (Munich, Germany) Novalis linear accelerator under calibration conditions. This calibration geometry included an SSD of 100 cm, 1.5 cm depth in solid water, 10 cm backscatter of solid water, and field size of 9.8 x 9.8 cm^2.

These setup parameters provide a dose rate of 1 cGy/MU according to the machine calibration setup. All of the calibration packets were delivered on the same day as the treatment TLD packets.

B. TLD Readout

The entire set of TLD packets for each fraction was kept together for approximately 24 hours before readout and were all read in the same session to reduce variability. TLD readings were performed on a REXON UL-320 TLD reader (Rexon Components, Inc., Beachwood, Ohio, USA). Each TLD packet was separated into three approximately equal samples of ~15 mg each. This was done in order to determine the mean dose and standard error of the mean for the TLD packets. The mass of each of the samples was taken prior to being placed into the TLD reader.

The TLD reader heated the samples to release the thermoluminescence and counted the number of photons released from the sample. This TL value was divided by the mass to obtain TL/mass of the sample. The average TL/mass of the unirradiated background samples was subtracted from the TL/mass of the calibration and treatment samples to provide $(TL/mass)_{net}$ for each.

The dose calibration factor (s_0) which converts $(TL/mass)_{net}$ to dose was obtained by taking the dose divided by $(TL/mass)_{net}$ at a dose of 2 Gy, as shown by the following equation.

$$s_0 = \left[\frac{dose}{(TL/mass)_{net}}\right]_{2\ Gy}$$

Using the factor s_0, each of the $(TL/mass)_{net}$ values from the calibration samples was converted into uncorrected dose values ($Dose_{uncorr}$).

$$Dose_{uncorr} = (TL/mass)_{net} * s_0$$

These values were plotted against their expected doses to obtain the non-linear correction factor (f_{lin}) from the dose calibration curve seen in Figure 2-16. The factor f_{lin} corrects the TLD doses for non-linearity. The non-linear correction factor was then applied to the uncorrected doses to obtain the corrected doses ($Dose_{corr}$).

$$Dose_{corr} = Dose_{uncorr} * f_{lin} = Dose_{uncorr} * slope + intercept$$

C. Delivery Verification and Dose Reconstruction

Since the RANDO phantom treatment was planned and delivered with TomoTherapy version 4.0.2.4, as opposed to version 3.x that had been used for each of the patients in this study, an updated version of the DVPA software had to be installed because the patient archive files have been altered in the new version. The Alpha-7 build of the DVPA software was installed which allowed for input of converted patient archives from TomoTherapy TPS version 4.x.

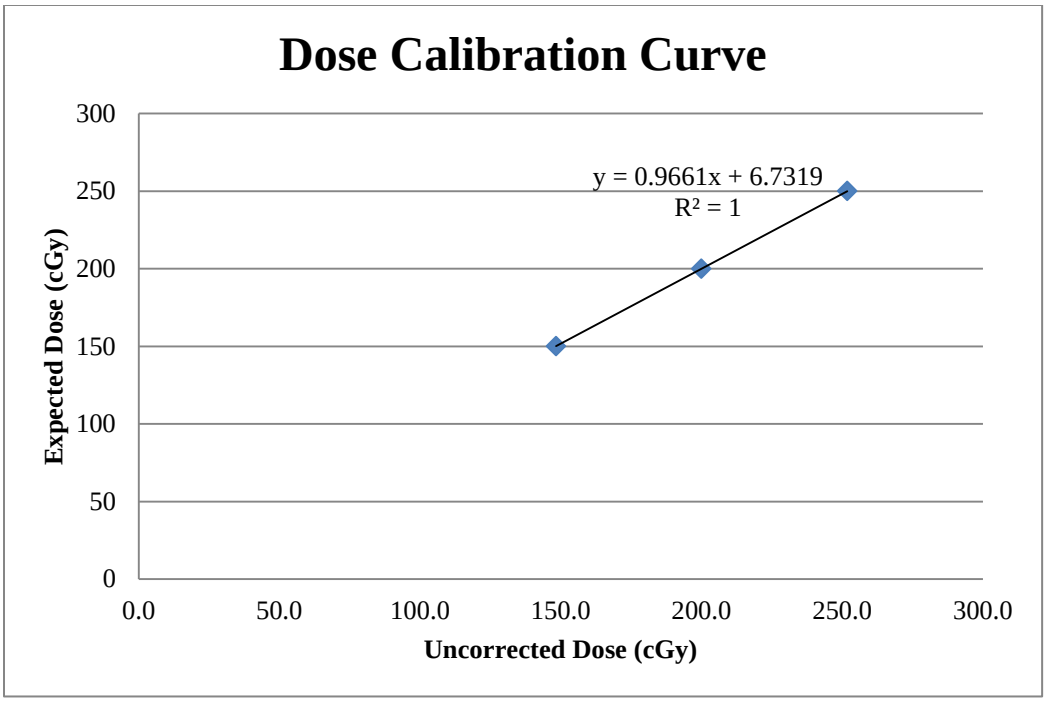

Figure 2-16: TLD Dose Calibration Curve and linear fit data

The updated version of the DVPA software had only minor cosmetic changes to the user interface, but all options were the same as the previous version. The database method was used with the phantom MVCT images and treatment exit detector data to reconstruct the delivered dose. The same options and methods were used for DV and DR as were used on the patient data in section 2-I-B.

Since the phantom delivery did not include any inter/intrafraction motion in the treatment, determination of the location of the TLD packets was more precise than with the patient treatment data. The reconstructed point dose at the TLD location was extracted from the DVPA software for comparison to the measured TLD doses.

D. Comparison of DVPA Doses and TLD Doses

Just as with the patient data (section 2-I-D), for all 3 fractions of phantom data acquired, the TLD dose and corresponding DVPA point doses were compared using the following

equation to calculate the percent difference (Δ(%)) between the two dose values:

$$\Delta(\%) = \frac{(T - D)}{T} * 100$$

Where T is the measured TLD dose and D is the reconstructed point dose from the DVPA software.

MATLAB software was used to show correlation between TLD doses and DVPA doses. Linear regression was performed using least-squares method on the data. The data was also fitted with 95% CI and 95% PI.

Chapter 3. Results

I. Aim 1

Results showing the comparison between the measured TLD doses and reconstructed DVPA doses for all five patients are shown in Figures 3-1 to 3-15. The doses and percent differences are plotted against fraction number. Error bars in the TLD dose graphs represent standard error of the mean for each TLD dose measurement, which was calculated from three samples of each TLD packet. Error bars in the DVPA dose graphs represent the standard error of the mean for each DVPA dose calculation as calculated from the estimated TLD location and the four surrounding points. The shaded region in the percent difference graphs defines the clinical acceptability range of ± 5% agreement [28]. A negative percent difference represents a TLD dose that is less than the DVPA dose. Error bars in the percent difference graph were calculated by combining the uncertainties from the TLD and DVPA doses as seen in the following equation, where σ_z is the combined uncertainty, x is the DVPA dose value, σ_x is the uncertainty in the DVPA dose, y is the TLD dose value, and σ_y is the uncertainty in the TLD dose.

$$\sigma_z = \sqrt{\left(\frac{100}{y} * \sigma_x\right)^2 + \left(\frac{100 * x}{y^2} * \sigma_y\right)^2}$$

This equation was obtained by combining the uncertainties of the percent difference formula described below where z represents the percent difference between two values x and y.

$$z = \frac{y - x}{y} * 100$$

A summary of the results for all five patients including average TLD dose, average DVPA dose, and average percent difference for each TLD location is shown in Tables 3-1 to 3-5. All doses shown are in cGy and the standard deviation of all values used to calculate the mean

are shown for each category. The percent difference values shown in the tables represent the average of all the percent differences calculated for each TLD location as well as the standard deviation of those values. The mean difference is the average of all values for each patient.

Table 3-1: Summary of dose results for patient A

Patient A			
TLD #	**TLD Dose (cGy)**	**DVPA Dose (cGy)**	**% Difference**
1	202.2 ± 5.2	205.0 ± 2.5	-1.4 ± 2.6
2	215.1 ± 9.0	214.7 ± 2.9	-0.1 ± 4.3
3	198.1 ± 8.5	206.2 ± 4.4	-4.2 ± 4.0
4	206.0 ± 8.1	205.9 ± 3.1	-0.5 ± 4.1
		Mean Difference	-1.6 ± 4.0

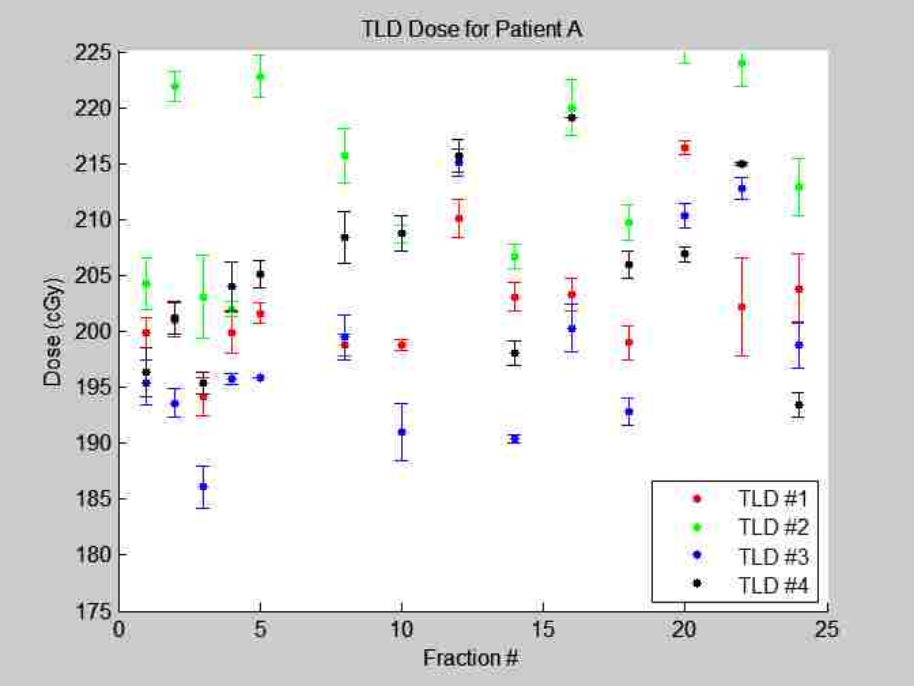

Figure 3-1: Data showing measured TLD doses per fraction for each location for patient A

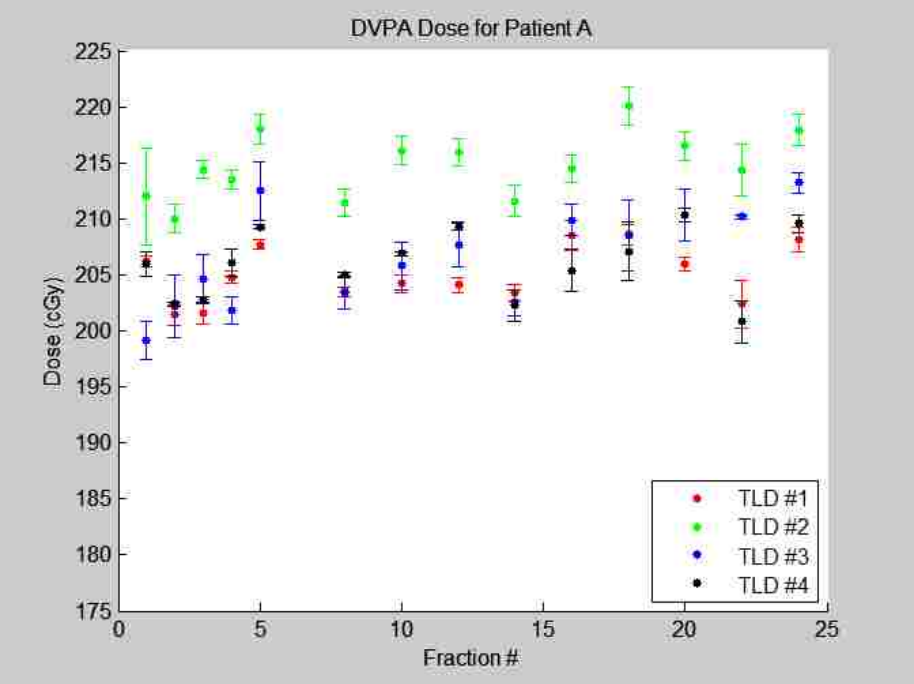

Figure 3-2: Data showing reconstructed DVPA doses per fraction for each location for patient A

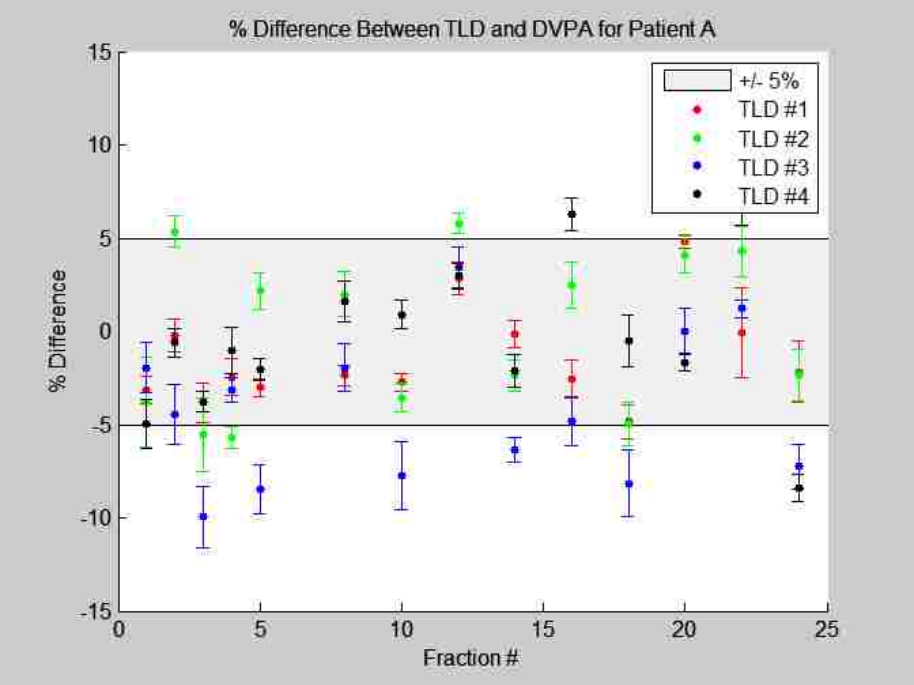

Figure 3-3: Data showing percent difference between TLD and DVPA doses for patient A

Table 3-2: Summary of dose results for patient B

Patient B			
TLD #	**TLD Dose (cGy)**	**DVPA Dose (cGy)**	**% Difference**
1	188.2 ± 9.1	198.1 ± 4.2	-5.5 ± 4.4
2	195.4 ± 5.4	200.4 ± 4.1	-2.6 ± 3.1
3	188.5 ± 5.9	191.1 ± 3.8	-1.5 ± 3.9
4	192.5 ± 4.6	195.7 ± 3.9	-1.7 ± 3.7
		Mean Difference	-2.8 ± 4.0

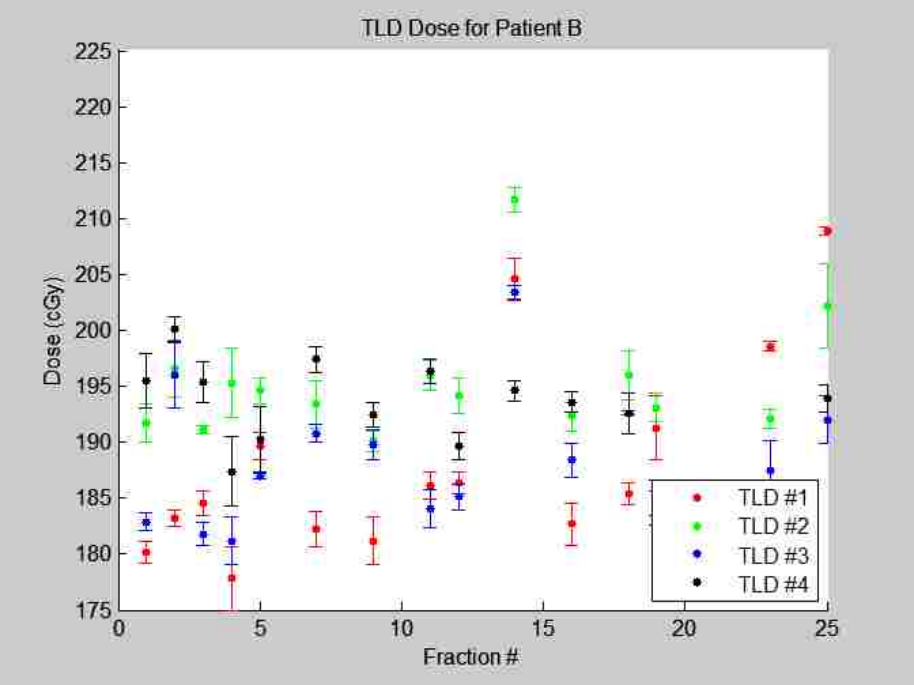

Figure 3-4: Data showing measured TLD doses per fraction for each location for patient B

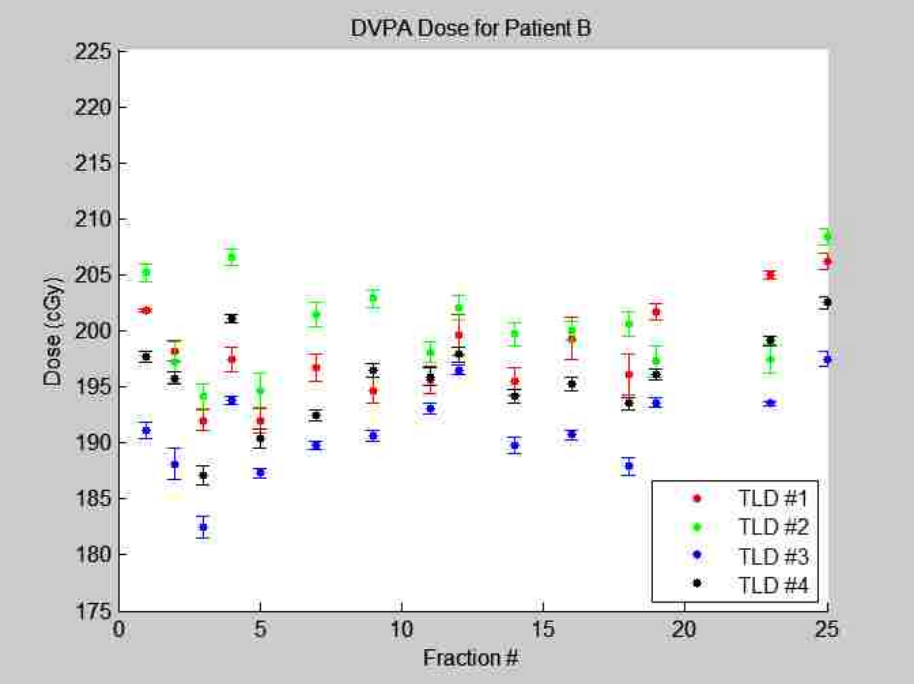

Figure 3-5: Data showing reconstructed DVPA doses per fraction for each location for patient B

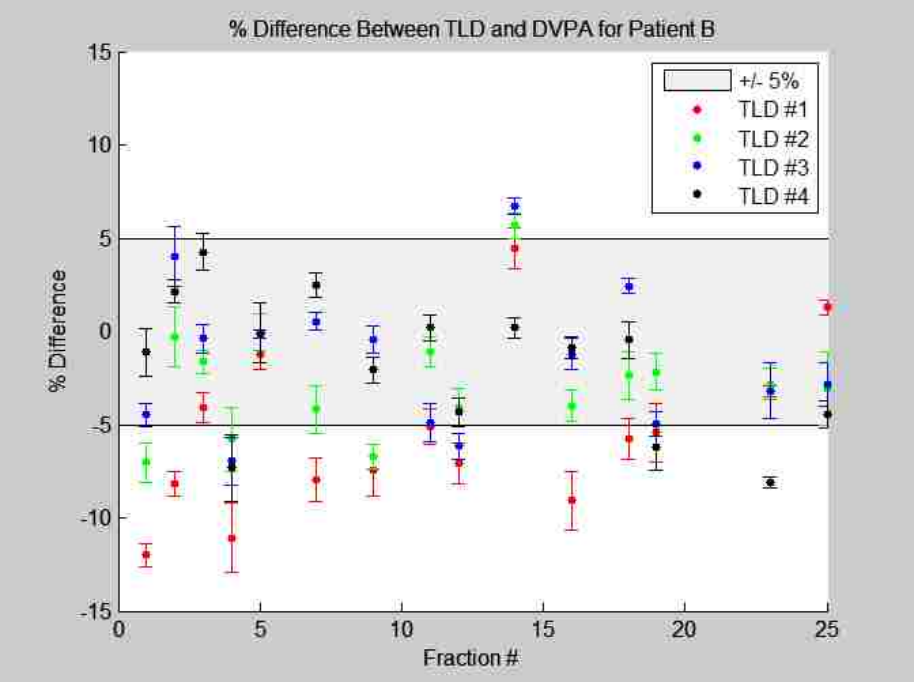

Figure 3-6: Data showing percent difference between TLD and DVPA doses for patient B

Table 3-3: Summary of dose results for patient C

Patient C			
TLD #	**TLD Dose (cGy)**	**DVPA Dose (cGy)**	**% Difference**
1	199.5 ± 5.6	202.0 ± 2.1	-1.6 ± 2.4
2	200.9 ± 7.3	200.0 ± 3.7	0.1 ± 3.2
3	203.8 ± 7.0	206.3 ± 4.4	-1.4 ± 3.7
4	205.1 ± 5.6	208.2 ± 3.9	-1.7 ± 3.6
		Mean Difference	-1.1 ± 3.3

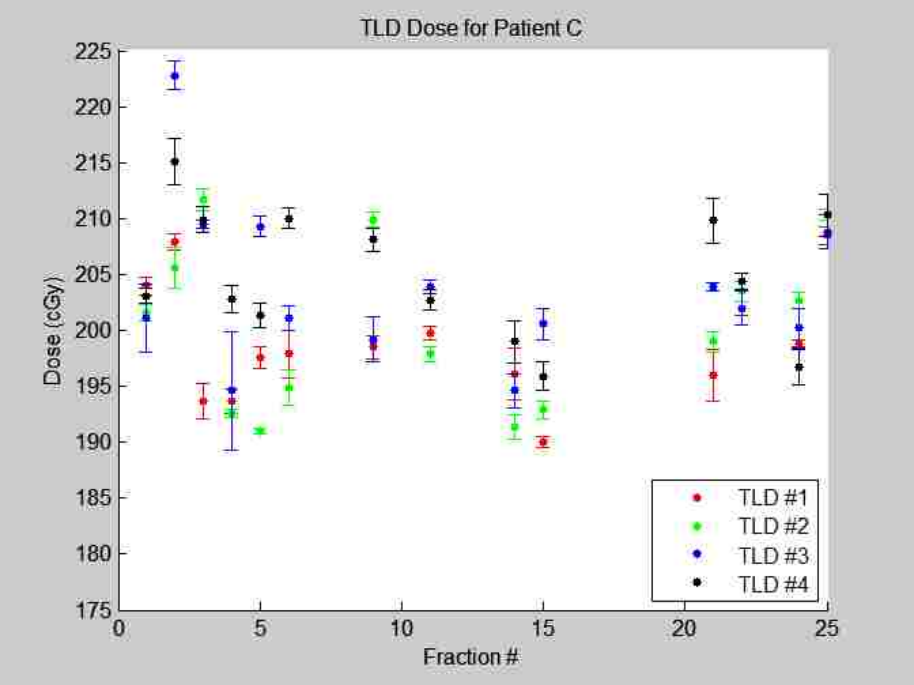

Figure 3-7: Data showing measured TLD doses per fraction for each location for patient C

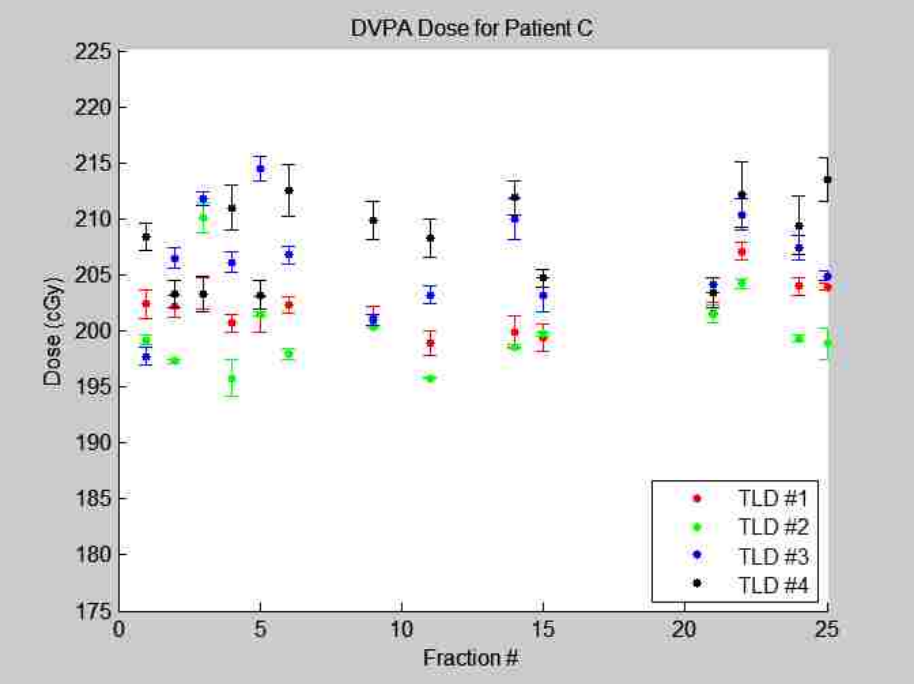

Figure 3-8: Data showing reconstructed DVPA doses per fraction for each location for patient C

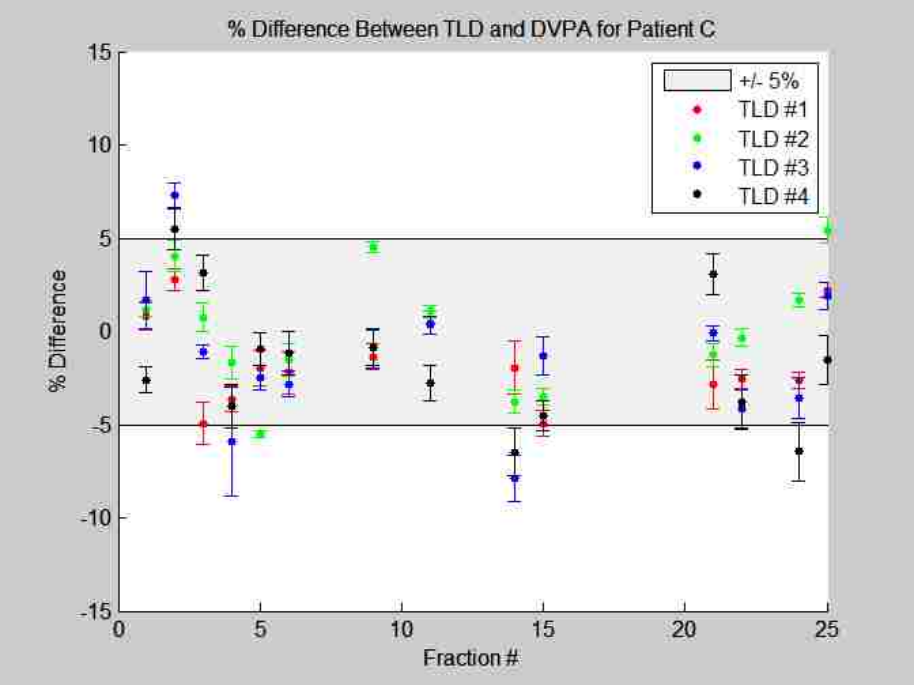

Figure 3-9: Data showing percent difference between TLD and DVPA doses for patient C

Table 3-4: Summary of dose results for patient D

Patient D			
TLD #	**TLD Dose (cGy)**	**DVPA Dose (cGy)**	**% Difference**
1	193.1 ± 8.1	206.0 ± 7.5	-7.3 ± 6.0
2	195.0 ± 8.4	200.4 ± 7.9	-3.0 ± 4.2
3	206.3 ± 6.4	209.7 ± 6.3	-1.8 ± 4.8
4	209.8 ± 9.3	214.0 ± 3.3	-2.5 ± 5.1
		Mean Difference	-3.6 ± 5.4

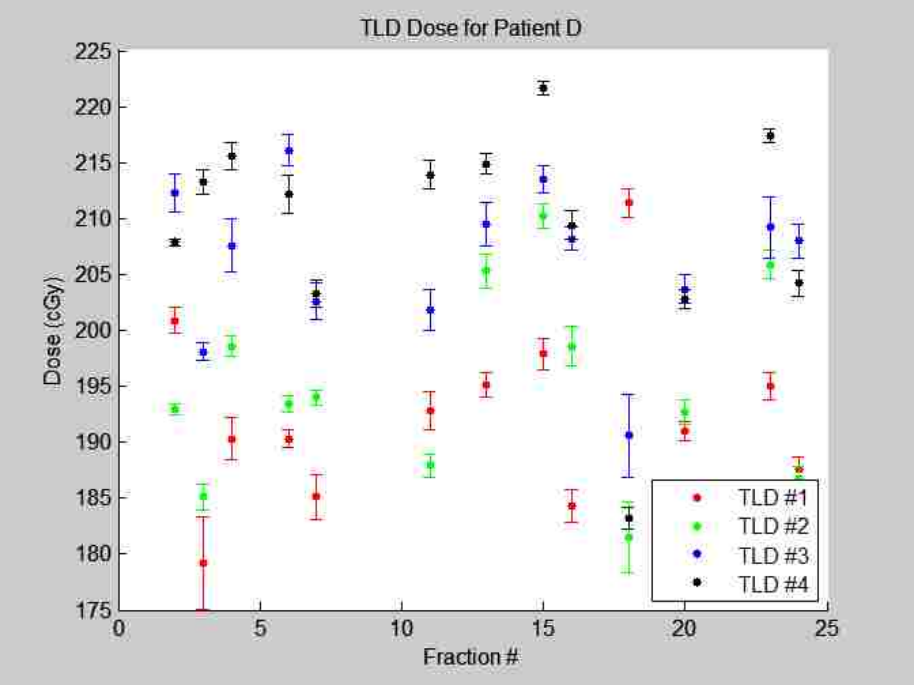

Figure 3-10: Data showing measured TLD doses per fraction for each location for patient D

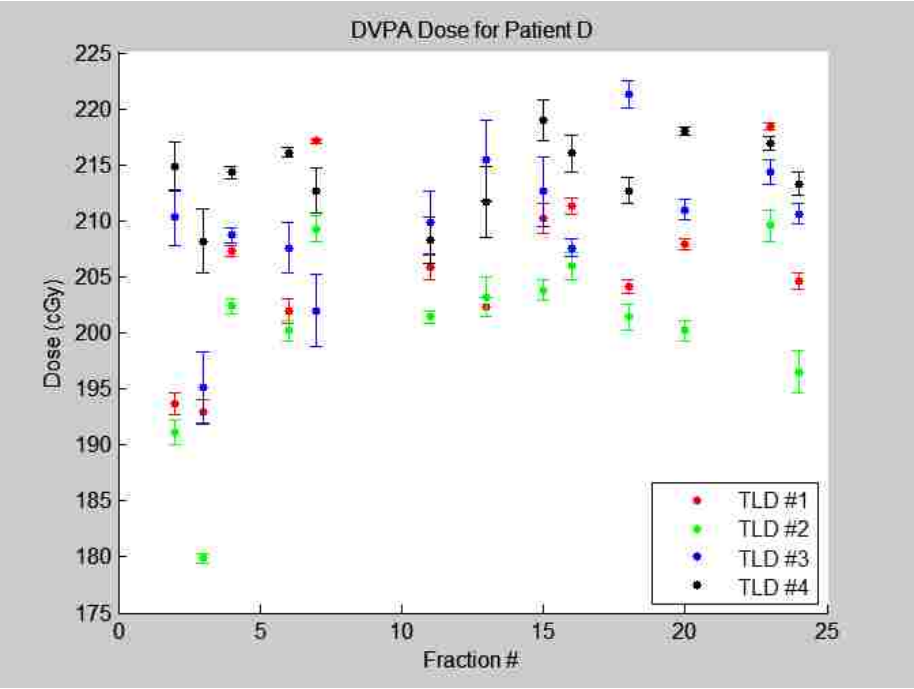

Figure 3-11: Data showing reconstructed DVPA doses per fraction for each location for patient D

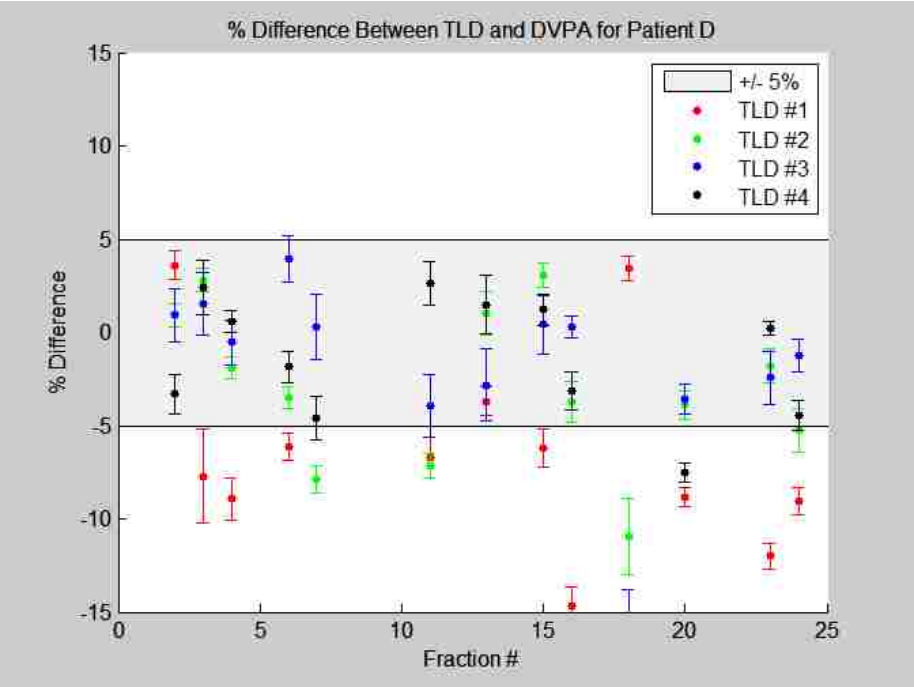

Figure 3-12: Data showing percent difference between TLD and DVPA doses for patient D

Table 3-5: Summary of dose results for patient E

Patient E			
TLD #	**TLD Dose (cGy)**	**DVPA Dose (cGy)**	**% Difference**
1	198.5 ± 6.4	211.1 ± 3.8	-6.5 ± 4.7
2	198.1 ± 7.7	215.4 ± 4.7	-8.9 ± 4.7
3	195.5 ± 5.8	206.7 ± 2.7	-5.9 ± 2.9
4	192.9 ± 9.3	201.9 ± 3.4	-5.0 ± 4.7
		Mean Difference	-6.6 ± 4.5

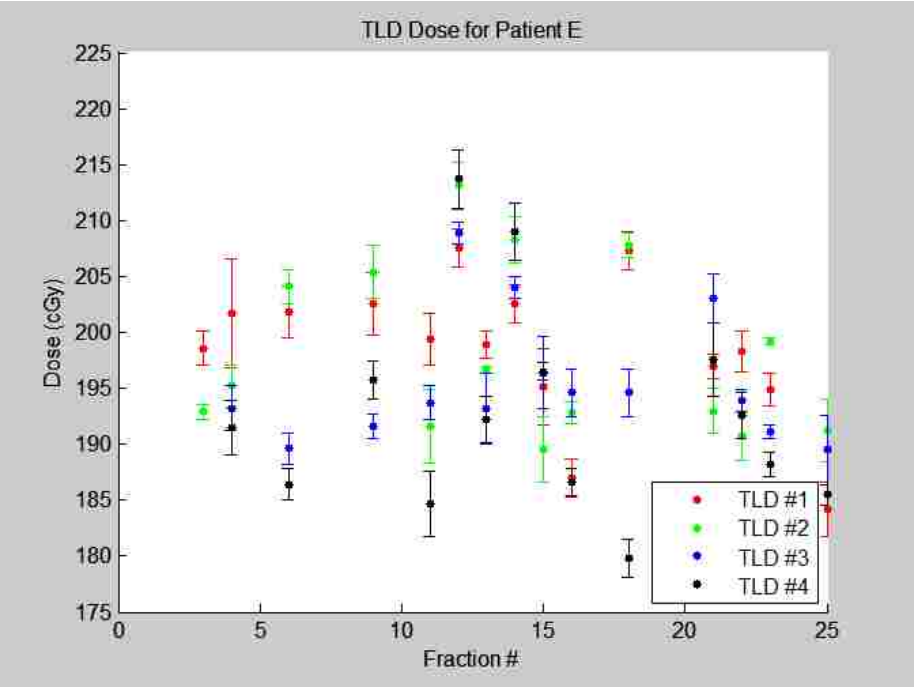

Figure 3-13: Data showing measured TLD doses per fraction for each location for patient E

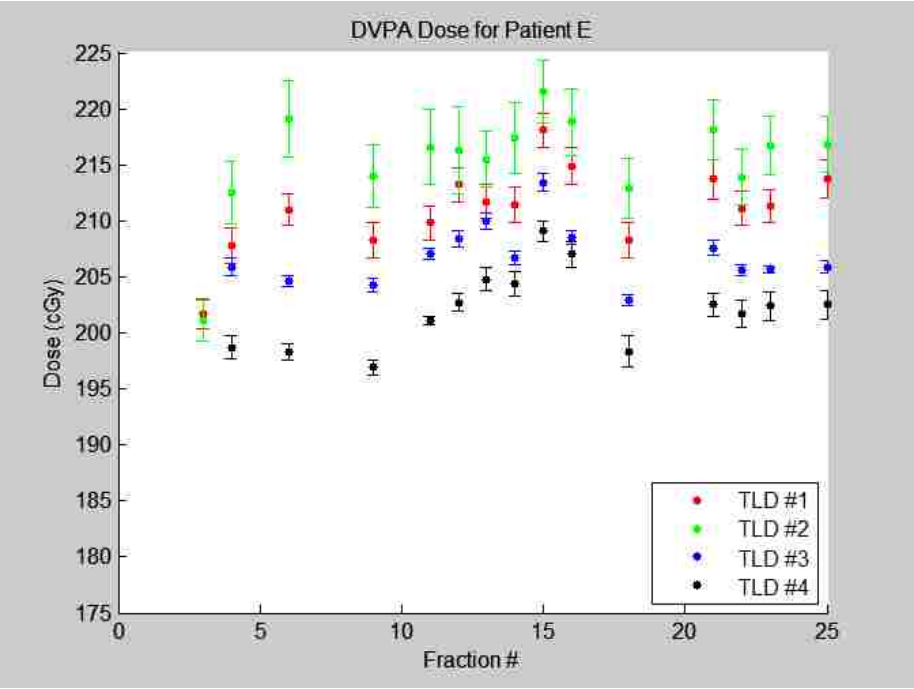

Figure 3-14: Data showing reconstructed DVPA doses per fraction for each location for patient E

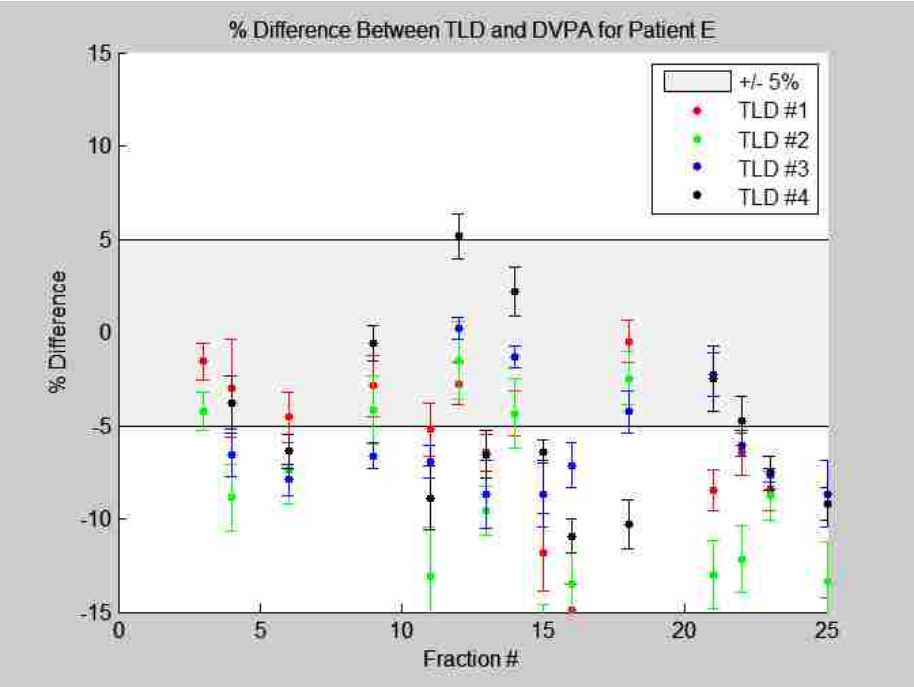

Figure 3-15: Data showing percent difference between TLD and DVPA doses for patient E

Table 3-6 shows the mean percent difference for each patient based on all TLD measurements and DVPA doses. Patient C had the best agreement between measured and reconstructed doses with mean differences of -1.1 ± 3.3 %. Only patient E had an overall difference outside of our clinical agreement criterion of 5%, and each of the TLD locations of patient E differed by more than 5%. Patients B and D each had one TLD location that differed by more than 5%, and all patients had several single measurements that differed by more than 5%. None of the patients had a TLD location with a difference of more than 10%. However, patients B, D, and E each had individual measurements that differed by more than 10%, with patient E having the most with 11 such measurements. All patients showed an overall negative percent difference meaning the measured TLD doses were lower than the reconstructed DVPA doses.

Table 3-7 shows the total number and percentage of points that fall outside of 5% and 10% as well as the maximum and minimum overall percent differences. The total number of valid measurement comparisons was 282 as seen in Table 2-1. The minimum of -17.8% was from patient D and the maximum of 7.3% was from patient C.

Table 3-6: Mean percent differences for each patient based on all of the measured and reconstructed doses

Patient	Mean Difference
A	-1.6 ± 4.0
B	-2.8 ± 4.0
C	-1.1 ± 3.3
D	-3.6 ± 5.4
E	-6.6 ± 4.5
All	-3.2 ± 4.7

The overall mean difference for all patients was calculated as the average of all measurements taken since each patient may have had a different number of measurements as seen in Table 2-1.

Table 3-7: Number and percentage of points that fell outside of specified ranges as well as max and min deviations

Number of points outside 5%:	95 of 298 (33.7%)
Number of points outside 10%:	19 of 298 (6.7%)
Max Deviation:	7.3%
Min Deviation:	-17.3%

The results in Figures 3-16 through 3-21 show the correlation between measured TLD doses and the corresponding reconstructed DVPA doses for patients A through E and the combination of all patients. Ideally, the TLD and DVPA doses would be equal for each data point resulting in a plot with a slope of 1 and y-intercept of 0. However, there appears to be both random and systematic fluctuations in both data sets that cause a poor correlation. The vertical error bars shown in the graphs represent the standard error of the mean for the TLD dose measurements. The horizontal error bars in the graphs represent the standard error of the mean for the DVPA dose calculations.

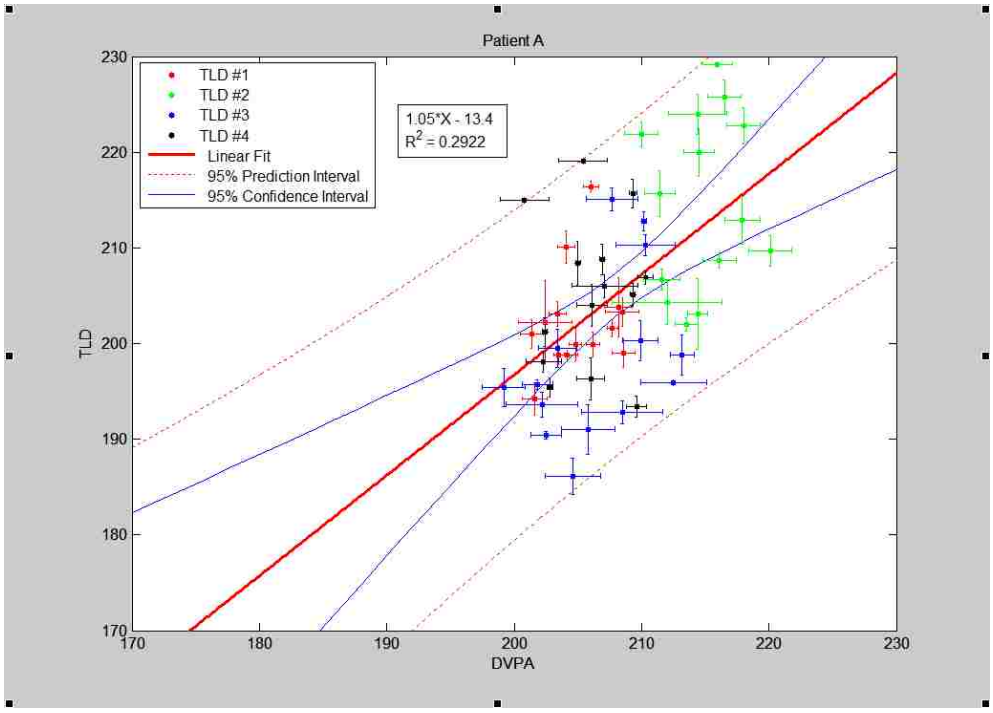

Figure 3-16: TLD doses vs. corresponding DVPA doses for patient A

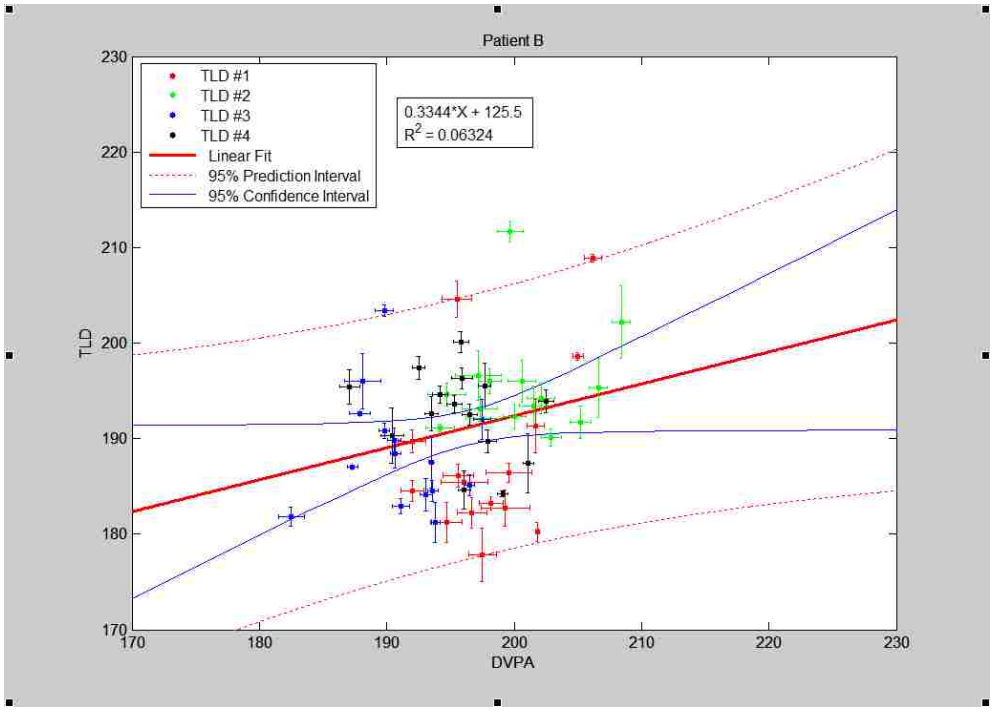

Figure 3-17: TLD doses vs. corresponding DVPA doses for patient B

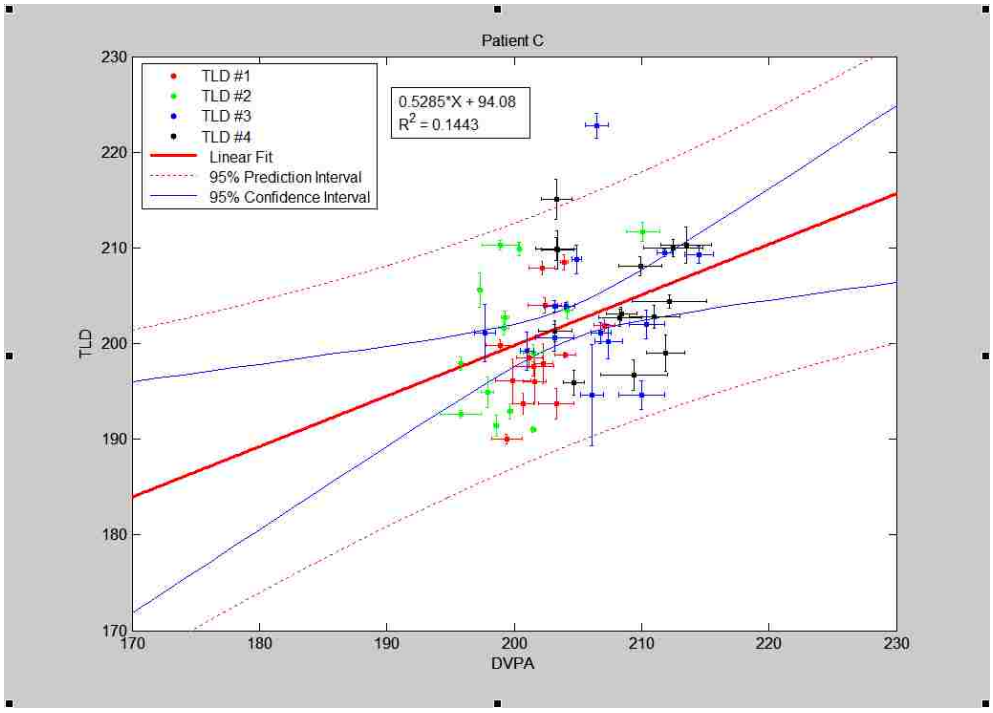

Figure 3-18: TLD doses vs. corresponding DVPA doses for patient C

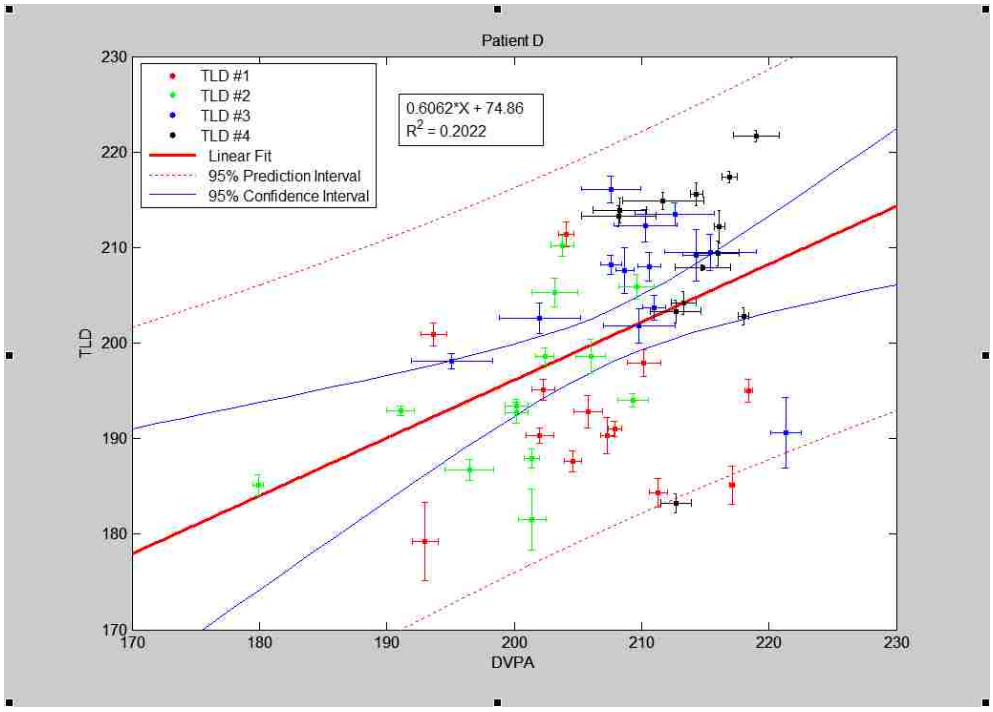

Figure 3-19: TLD doses vs. corresponding DVPA doses for patient D

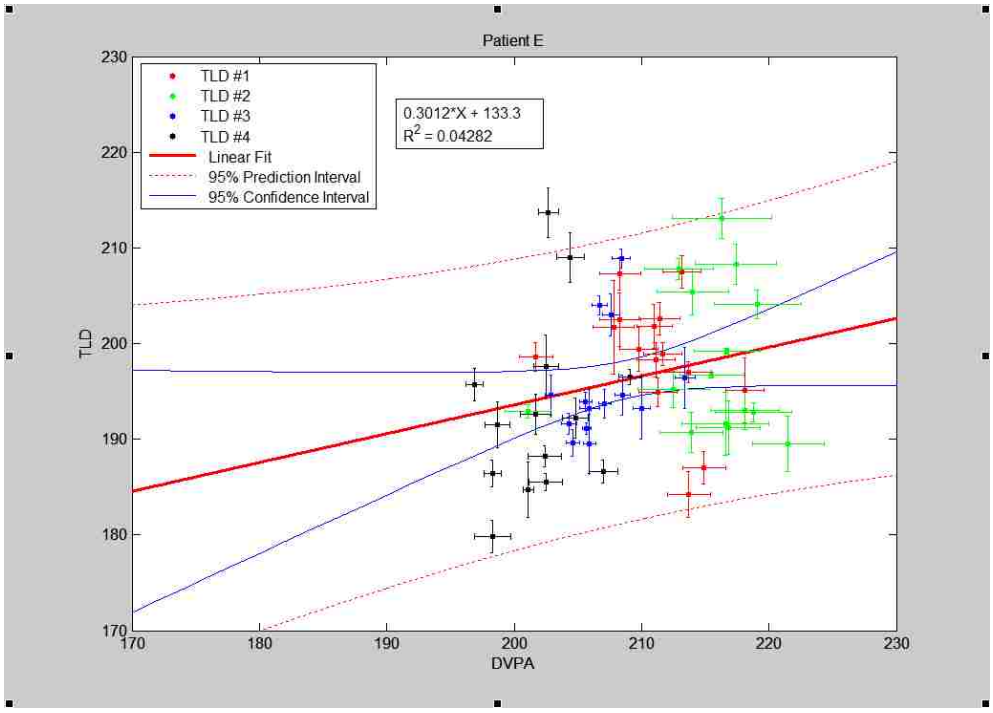

Figure 3-20: TLD doses vs. corresponding DVPA doses for patient E

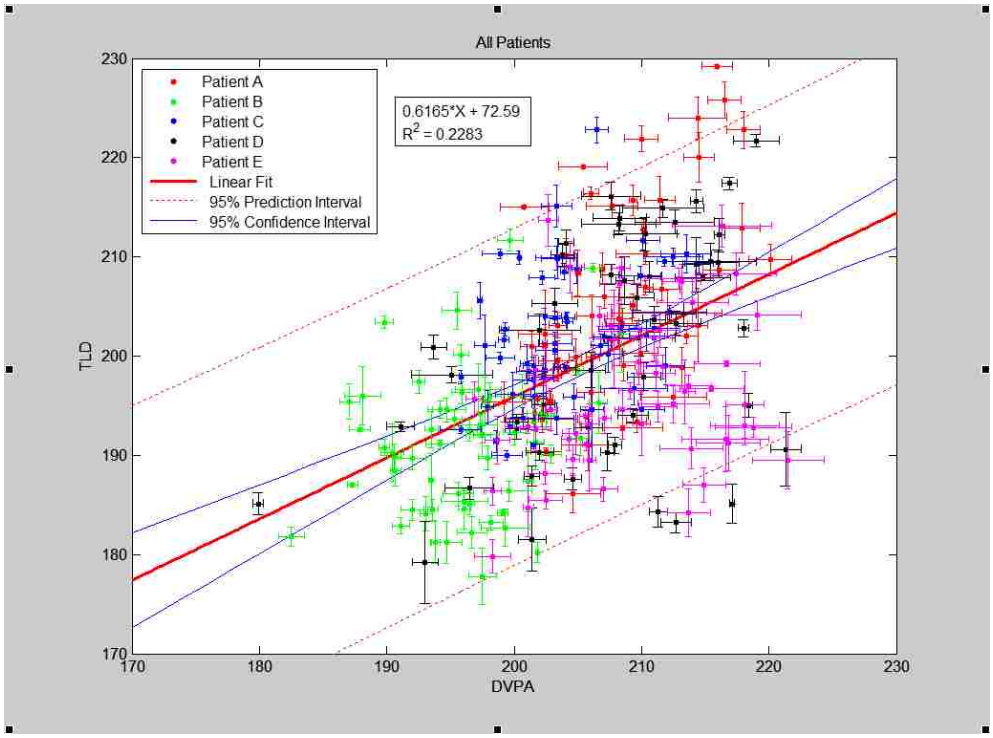

Figure 3-21: TLD doses vs. corresponding DVPA doses for all patients

A summary of the fit and correlation results from Figures 3-16 through 3-21 can be seen in Table 3-8. The best correlation and fit data was from patient A, which was closest to the ideal slope and y-intercept values of 1 and 0 respectively. Patient A also had a good agreement in the percent difference data with a mean difference of -1.6 ± 4.0 % (Table 3-6). However, the R^2 value for patient A was only 0.29 which does not show a good correlation. Patients B and E had the worst correlation and also showed very poor agreement in the percent difference data. The combination of all 282 data points from all patients had an R^2 value of 0.23. Since the levels of uncertainty were of the same order as the spread of data, the correlation of the linear relationship in this instance suffered. The poor correlation was not necessarily representative of a non-existent relationship between TLD and DVPA doses, but instead may represent the fact that there was poor agreement in individual points due to the relatively high uncertainty in the TLD doses.

Table 3-8: Linear fit and correlation results from the TLD vs. DVPA doses in Figures 3-16 through 3-21

	Linear Fit		95% C.I.		
Patient	**Slope**	**Intercept**	**Slope**	**Intercept**	**R^2**
A	1.05	-13.4	0.60 to 1.50	-106.2 to 79.5	0.29
B	0.33	125.5	0.00 to 0.67	59.1 to 191.9	0.06
C	0.53	94.1	0.18 to 0.88	22.4 to 165.8	0.14
D	0.61	74.9	0.26 to 0.95	3.8 to 145.9	0.20
E	0.30	133.3	-0.02 to 0.62	66.4 to 200.3	0.06
All	0.62	72.6	0.48 to 0.75	45.3 to 99.9	0.23

II. Aim 2

The results of the TomoTherapy PMRT treatment plan on the RANDO phantom can be seen in the following dose distributions and dose volume histogram (DVH) in Figures 3-22

through 3-24. The goal was to create a plan that is similar in terms of dose conformity to the PTV and dose avoidance to organs at risk (OAR) to a typical treatment plan delivered clinically to a patient undergoing PMRT with TomoTherapy.

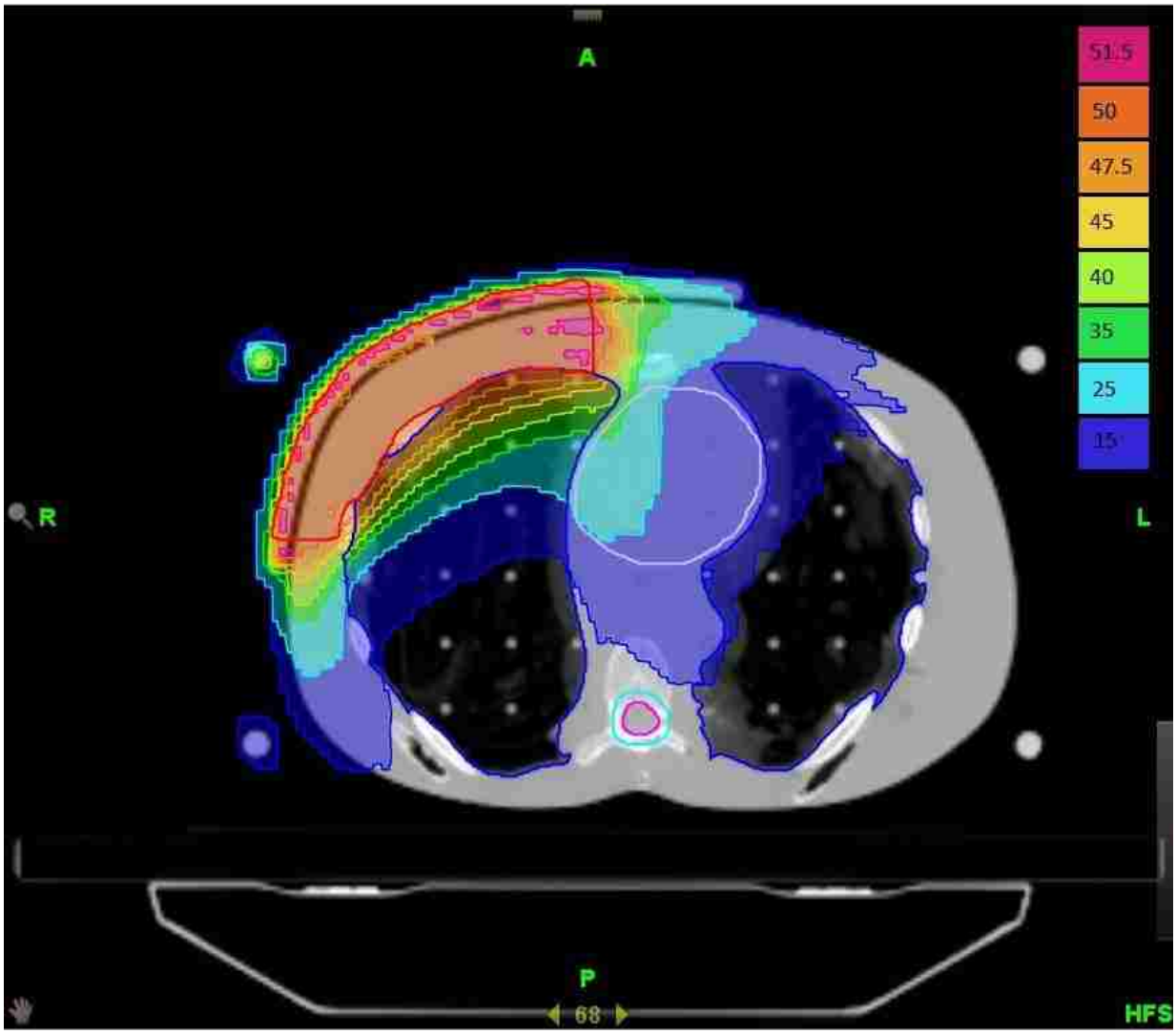

Figure 3-22: Transverse view of the planned dose distribution in the RANDO phantom

The PMRT plan created for the RANDO phantom is shown to be very similar to the plans used in the planning study by Ashenafi et al. (Figure 1-6) as well as plans that are delivered clinically at MBPCC in terms of dose coverage and homogeneity to the PTV as well as normal

tissue and critical structure dose sparing. The dose in the chestwall PTV is homogeneous at the planned dose of 50 Gy. Outside of the PTV there is a sharp dose falloff with minimal doses being delivered to the OARs including the heart, lungs, and spinal cord. As is the case in many TomoTherapy treatments a relatively large volume of the patient receives a low dose.

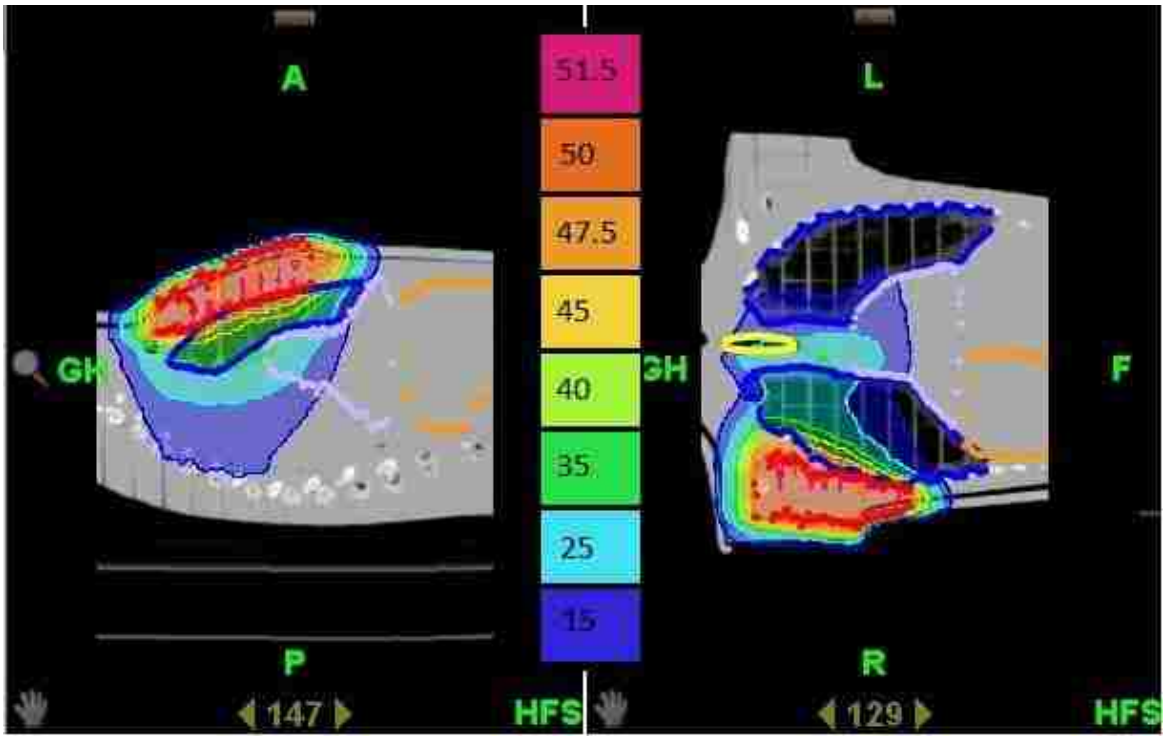

Figure 3-23: Sagittal and coronal views of the planned dose distribution in the RANDO phantom

The dose volume histogram (DVH) (Figure 3-24) shows that most of the metrics used to create the plan were met in order to achieve minimum doses to the OARs. Also, the sharp dose falloff in the red line of the chestwall PTV shows a homogeneous dose is being achieved inside the PTV, as 93% of the PTV receives 50 Gy, 99% receives 48.4 Gy, and 1% receives 52.2 Gy. This uniform dose is slightly better than a typical clinical PMRT case. The final treatment time (4.6 minutes) and modulation factor (2.8) were comparable to clinical plans.

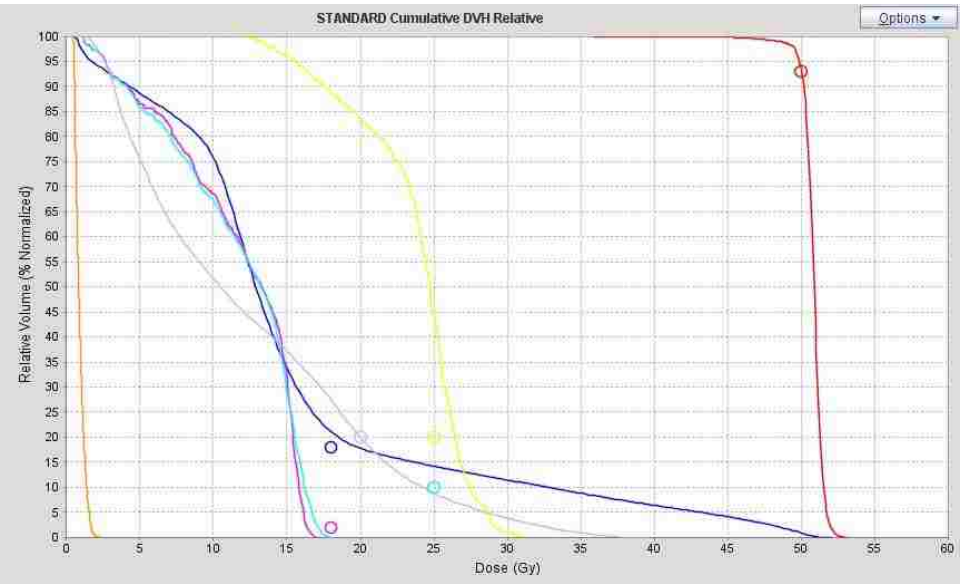

Figure 3-24: Dose Volume Histogram for the TomoTherapy PMRT treatment to the RANDO phantom (Red – Chestwall PTV, Yellow – Airway, Blue – Lungs, Violet – Heart, Pink – Spinal Cord, Orange – Liver)

III. Aim 3

Comparisons between the measured TLD doses and reconstructed DVPA doses which were calculated from the MVCT for the RANDO phantom treatments are shown in Figures 3-25 to 3-30. The phantom had 8 TLD locations surrounding the mastectomy scar-tape on the chest wall surface. The doses and percent difference are plotted against fraction number for each TLD location and for each of the three treatment deliveries. Error bars in the TLD dose graphs represent standard error of the mean for each TLD dose measurement, which was calculated from three samples of each TLD packet. The shaded region in the percent difference graphs is the standard clinical acceptability criteria of ± 5%. A positive percent difference represents a TLD dose that is greater than the DVPA dose. The error bars in the percent difference graphs represent the fractional standard error of the mean of the TLD dose measurements. Only one DVPA dose value was calculated for each TLD location on the phantom so uncertainty estimates are unavailable for those.

A summary of the results for the RANDO phantom treatment including average TLD dose, average DVPA dose from the MVCT images, and average percent difference for each TLD location is shown in Table 3-9. Table 3-10 shows the values for each quantity presented as the average of all eight measurement (or calculation) locations for each of the three treatment deliveries. All doses shown are in cGy and the standard deviation of all values used to calculate the mean is shown for each category.

Table 3-9: Summary of dose results for the RANDO phantom organized by TLD location. The DVPA doses were calculated from MVCT images.

TLD #	TLD Dose (cGy)	DVPA Dose (cGy)	% Difference
1	197.6 ± 3.5	189.5 ± 1.1	4.1 ± 1.6
2	199.0 ± 4.1	184.9 ± 0.6	7.0 ± 2.0
3	195.8 ± 5.5	188.1 ± 0.5	3.9 ± 2.5
4	201.2 ± 4.0	191.3 ± 1.2	4.9 ± 2.2
5	195.2 ± 6.5	189.6 ± 1.0	2.8 ± 3.5
6	191.6 ± 3.0	187.1 ± 1.1	2.3 ± 1.7
7	195.9 ± 6.9	187.3 ± 0.8	4.3 ± 3.2
8	192.5 ± 4.5	189.5 ± 0.9	1.6 ± 2.4
		Mean Difference	3.9 ± 2.6

Table 3-10: Summary of dose results for the RANDO phantom organized by treatment fraction number. The DVPA doses were calculated from MVCT images.

Fx #	TLD Dose (cGy)	DVPA Dose (cGy)	% Difference
1	197.3 ± 4.2	187.5 ± 1.8	5.0 ± 2.1
2	191.3 ± 3.5	188.6 ± 2.1	1.4 ± 2.1
3	199.7 ± 3.5	189.2 ± 2.0	5.2 ± 1.8
		Mean Difference	3.9 ± 2.6

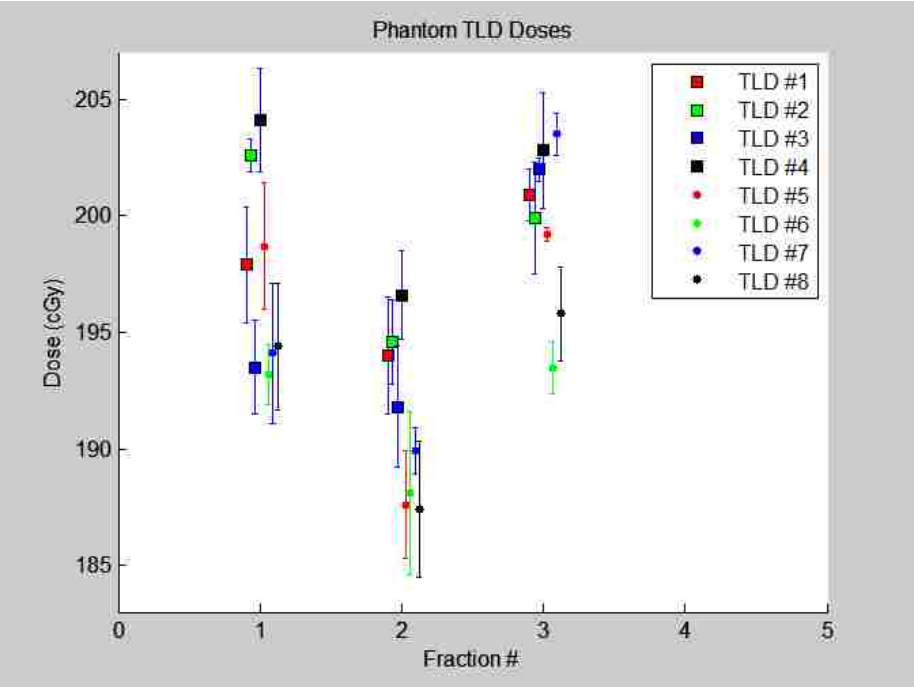

Figure 3-25: Phantom TLD doses at each TLD location

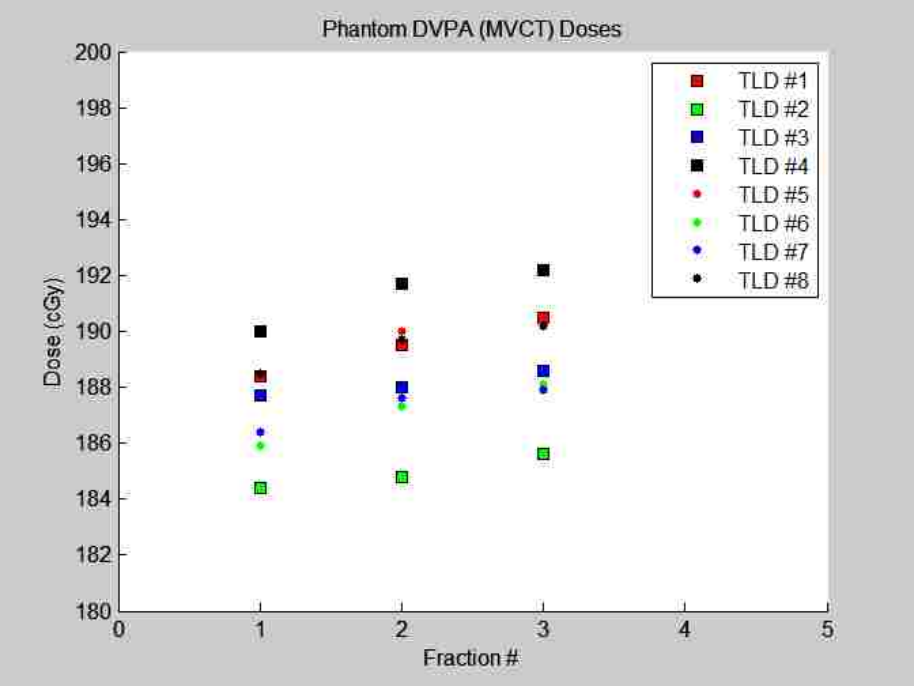

Figure 3-26: Phantom DVPA doses at each TLD location calculated from the MVCT

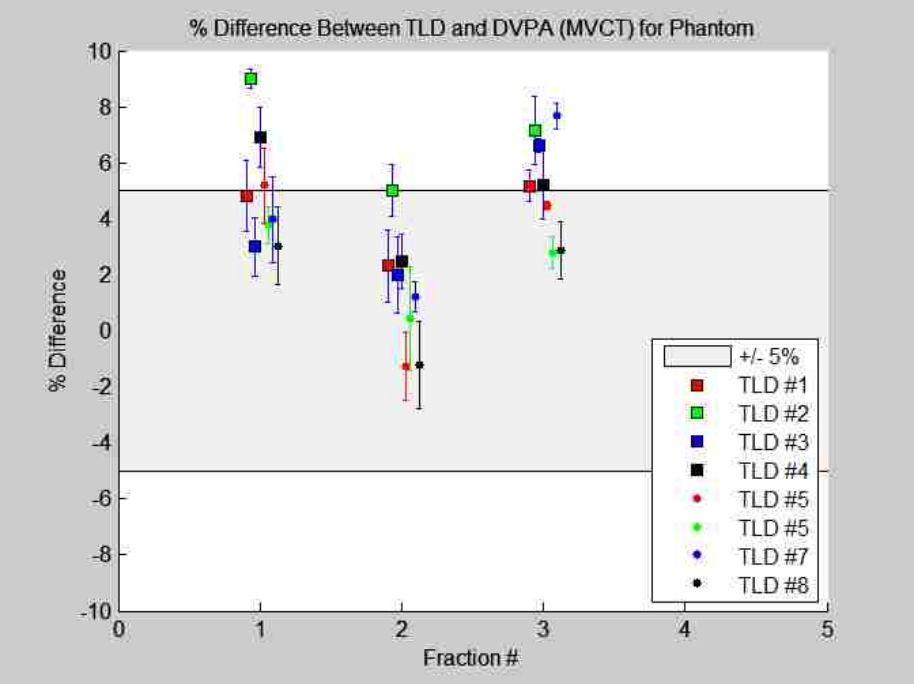

Figure 3-27: Percent difference between TLD and DVPA doses at each TLD location on the RANDO phantom for DVPA doses calculated from the MVCT

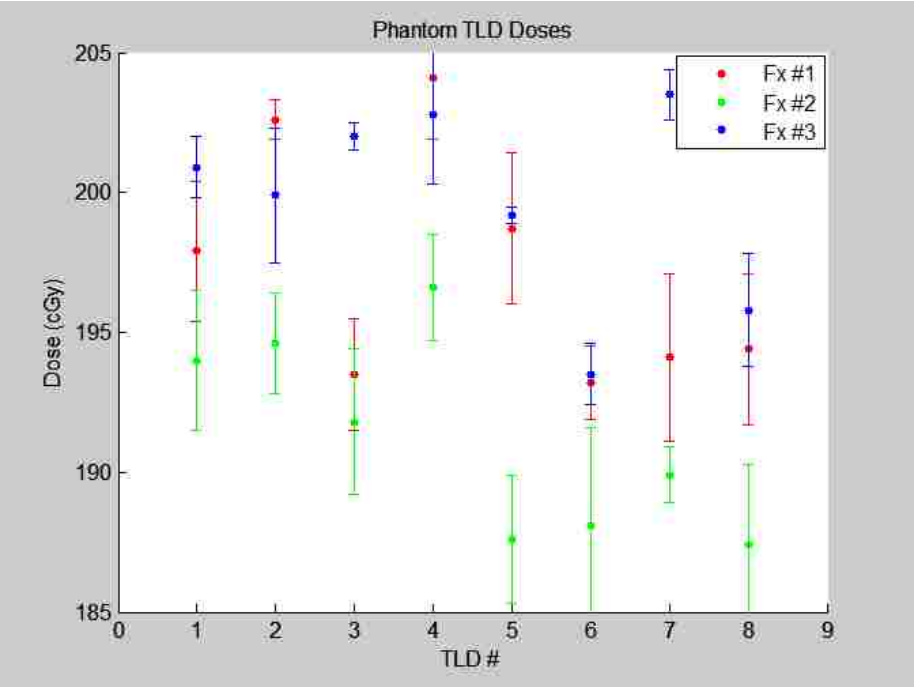

Figure 3-28: Phantom TLD doses for each treatment fraction

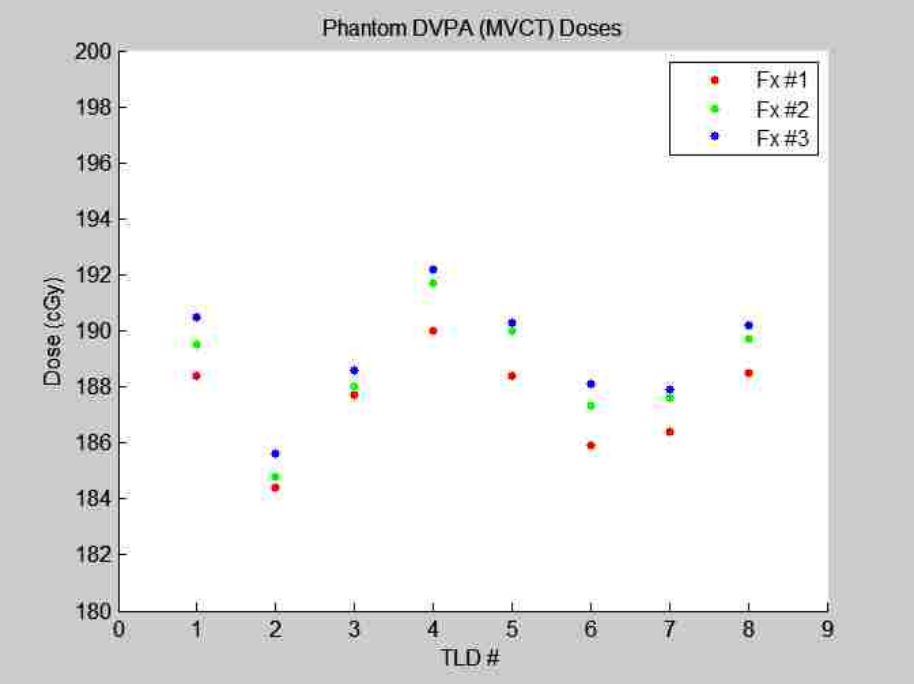

Figure 3-29: Phantom DVPA doses for each treatment fraction calculated from the MVCT

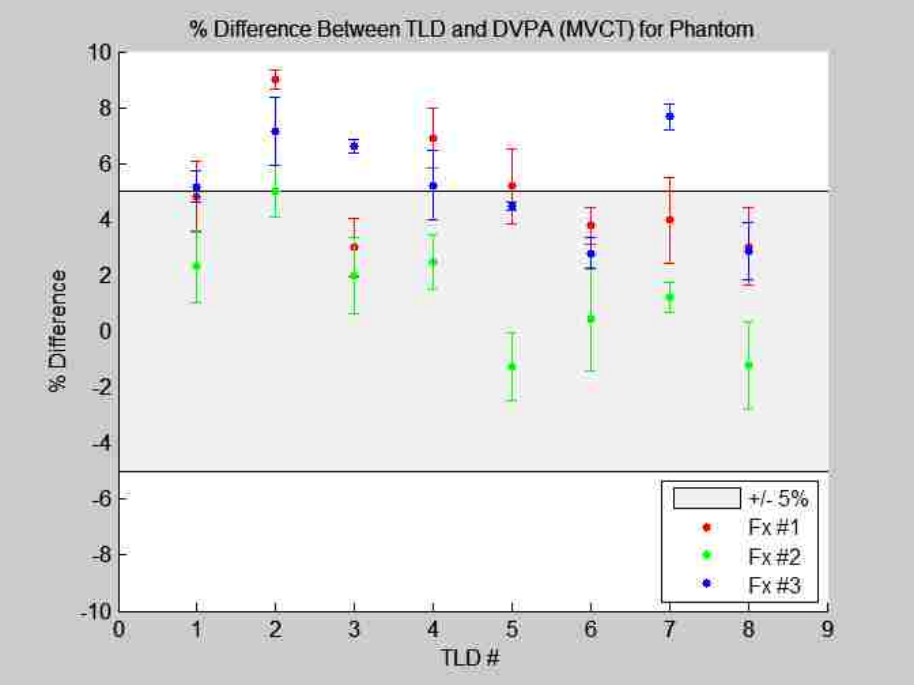

Figure 3-30: Percent difference between TLD and DVPA for each treatment fraction on the RANDO phantom for DVPA doses calculated from the MVCT

When the DVPA doses were calculated from the MVCT images, it was noticed that there seemed to be a systematic shift in the dose values and percent difference comparisons away from expected doses. This may have been caused by inaccurate values in the image value to density table (IVDT) which relates pixel values in the MVCT images to the physical density of the material in order to use in the dose calculations. To see whether this was the case, the DVPA doses were also calculated using the original kVCT images. Since the kVCT images were used in the calculation of the original plan, the recalculated doses should match the planned doses exactly when the planned sinogram is used. The DV sinogram was calculated from the database method and used to calculate dose on the kVCT images. This could be done in the phantom study due to the fact that the anatomy and setup remained the same without any interfraction or intrafraction changes.

The results of calculating the DVPA doses from kVCT images can be seen in figures 3-31 to 3-36. Table 3-11 gives a summary of the results for the RANDO phantom treatment including average TLD dose, average DVPA dose from the kVCT images, and average percent difference for each TLD location. Table 3-12 shows the values for each quantity presented as the average of all eight measurement (or calculation) locations for each of the three treatment deliveries. All doses shown are in cGy and the standard deviation of all values used to calculate the mean is shown for each category.

Table 3-13 shows the total number and percentage of points that fall outside of the 5% and 10% ranges as well as the maximum and minimum overall percent differences for DVPA doses calculated from the MVCT images. Table 3-14 shows the same comparisons for DVPA doses calculated from kVCT images. For each case the total number of valid measurement comparisons was 24 from a total of 8 TLD locations and 3 treatment fractions. In Table 3-13,

the minimum of -1.3 was from TLD #8 in fraction #2, and the maximum of 9.0 was from TLD #2 in fraction #1. In Table 3-14, the minimum and maximum values changed, but they remained from the same TLD location and delivery fraction number. The minimum of -5.2% was from TLD #8 in fraction #2, and the maximum of 5.4% was from TLD #2 in fraction #1.

Table 3-11: Summary of dose results for the RANDO phantom organized by TLD location. The DVPA doses were calculated from kVCT images.

TLD #	TLD Dose (cGy)	DVPA Dose (cGy)	% Difference
1	197.6 ± 3.5	196.1 ± 0.6	0.7 ± 2.0
2	199.0 ± 4.1	191.5 ± 0.7	3.7 ± 2.2
3	195.8 ± 5.5	195.5 ± 0.7	0.1 ± 3.1
4	201.2 ± 4.0	198.1 ± 1.0	1.5 ± 2.5
5	195.2 ± 6.5	194.2 ± 0.9	0.4 ± 3.8
6	191.6 ± 3.0	193.0 ± 1.1	-0.7 ± 2.1
7	195.9 ± 6.9	193.6 ± 0.6	1.1 ± 3.7
8	192.5 ± 4.5	196.2 ± 0.9	-2.0 ± 2.9
		Mean Difference	0.6 ± 2.9

Table 3-12: Summary of dose results for the RANDO phantom organized by treatment fraction number. The DVPA doses were calculated from kVCT images.

Fx #	TLD Dose (cGy)	DVPA Dose (cGy)	% Difference
1	197.3 ± 4.2	194.3 ± 2.0	1.5 ± 2.2
2	191.3 ± 3.5	195.6 ± 2.2	-2.3 ± 1.9
3	199.7 ± 3.5	194.4 ± 2.2	2.6 ± 1.8
		Mean Difference	0.6 ± 2.9

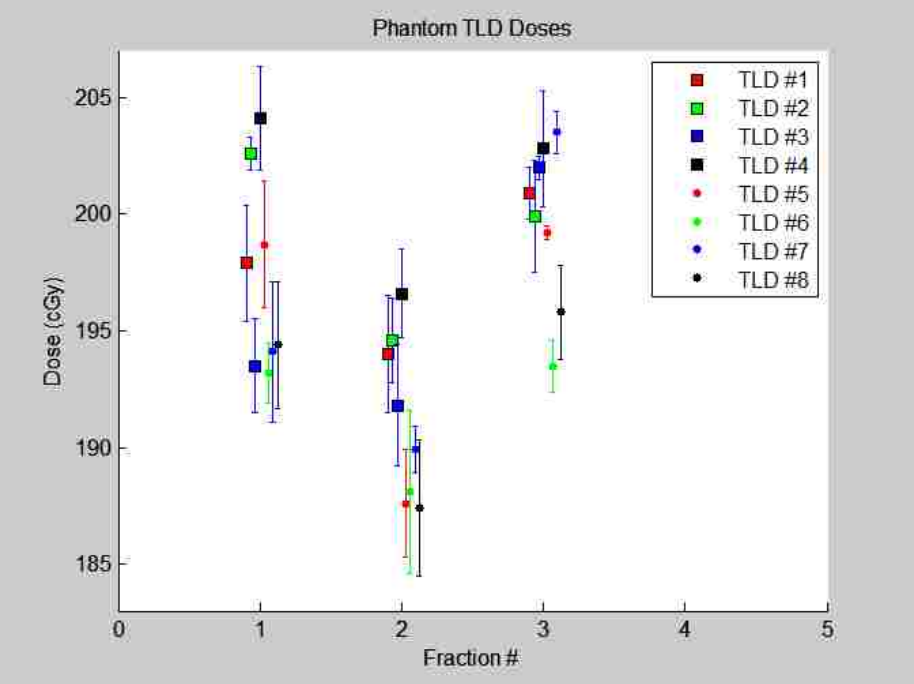

Figure 3-31: Phantom TLD doses at each TLD location

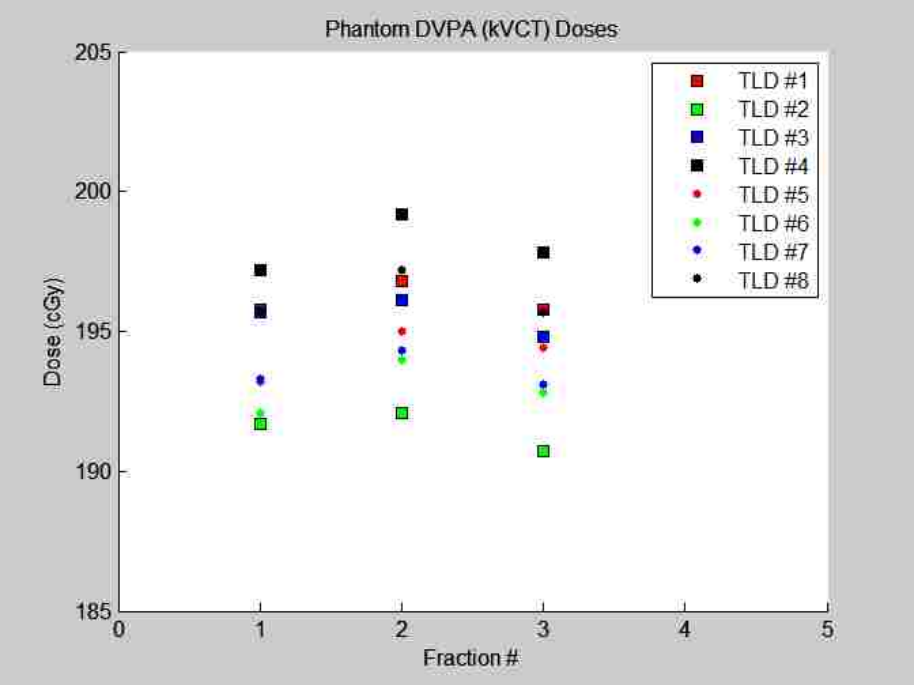

Figure 3-32: Phantom DVPA doses at each TLD location calculated from the kVCT

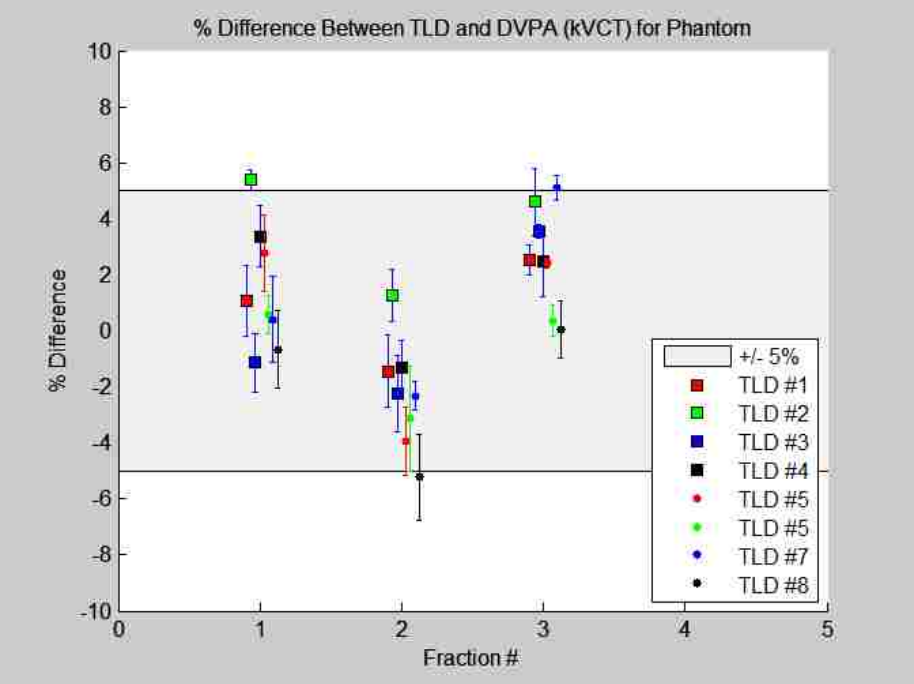

Figure 3-33: Percent difference between TLD and DVPA doses at each TLD location on the RANDO phantom for DVPA doses calculated from the kVCT

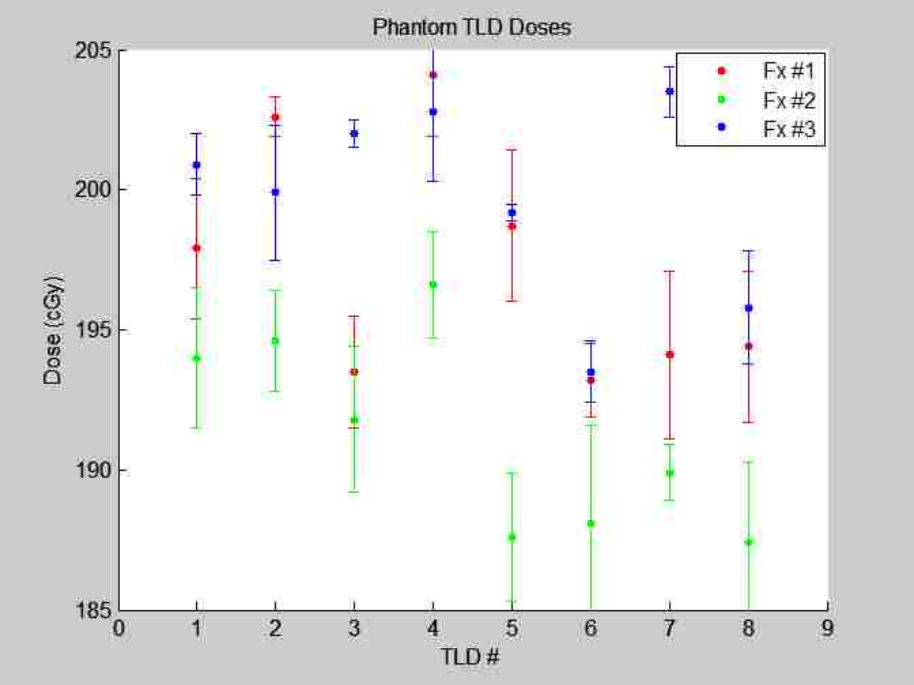

Figure 3-34: Phantom TLD doses for each treatment fraction

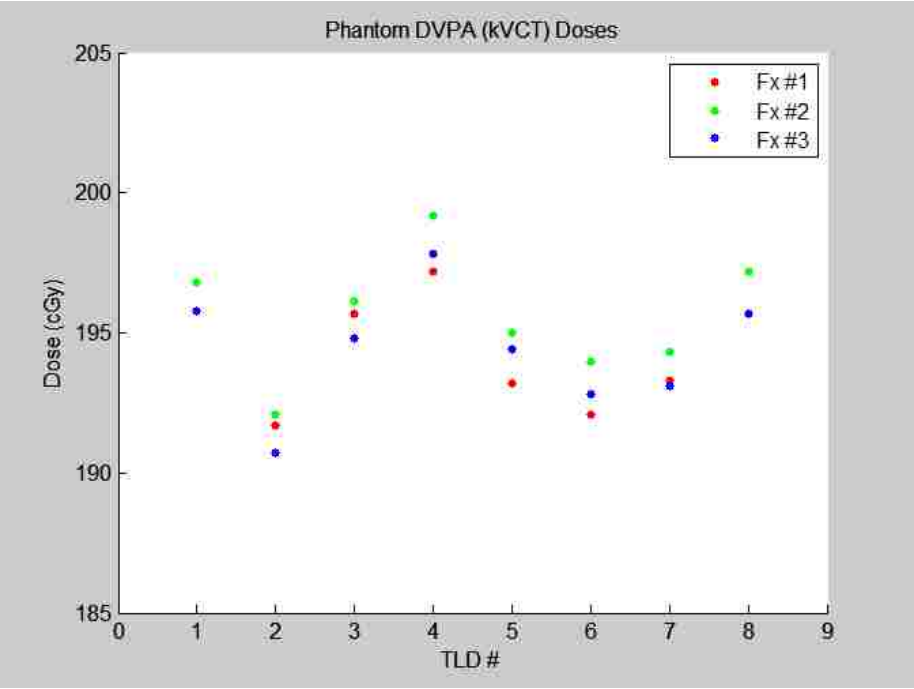

Figure 3-35: Phantom DVPA doses for each treatment fraction calculated from the kVCT

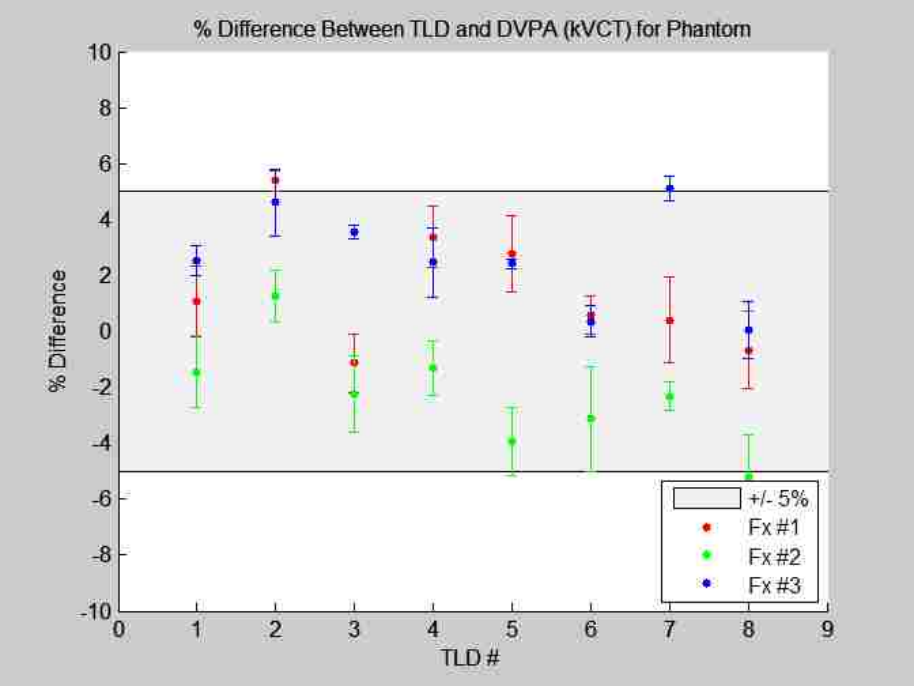

Figure 3-36: Percent difference between TLD and DVPA for each treatment fraction on the RANDO phantom for DVPA doses calculated from the kVCT

Table 3-13: Number and percentage of points that fell outside of specified ranges as well as max and min deviations for the RANDO phantom for DVPA doses calculated from the MVCT

Number of points outside 5%:	9 of 24 (37.5%)
Number of points outside 10%:	0 of 24 (0%)
Max Deviation:	9.0%
Min Deviation:	-1.3%

Table 3-14: Number and percentage of points that fell outside of specified ranges as well as max and min deviations for the RANDO phantom for DVPA doses calculated from the kVCT

Number of points outside 5%:	3 of 24 (12.5%)
Number of points outside 10%:	0 of 24 (0%)
Max Deviation:	5.4%
Min Deviation:	-5.2%

The results in Figures 3-37 and 3-38 show the correlation between measured TLD doses and the corresponding reconstructed DVPA doses (calculated from the MVCT images) for the RANDO phantom. The data is organized by TLD location as well as fraction number. Ideally, the TLD and DVPA doses would be equal for each data point resulting in a plot with a slope of 1 and y-intercept of 0. However, there appears to be both random and systematic fluctuations in both data sets that cause a poor correlation. The error bars shown in the graphs represent the standard error of the mean for the TLD dose measurements. Figures 3-39 and 3-40 show the same comparison for the DVPA doses that were calculated from the kVCT images.

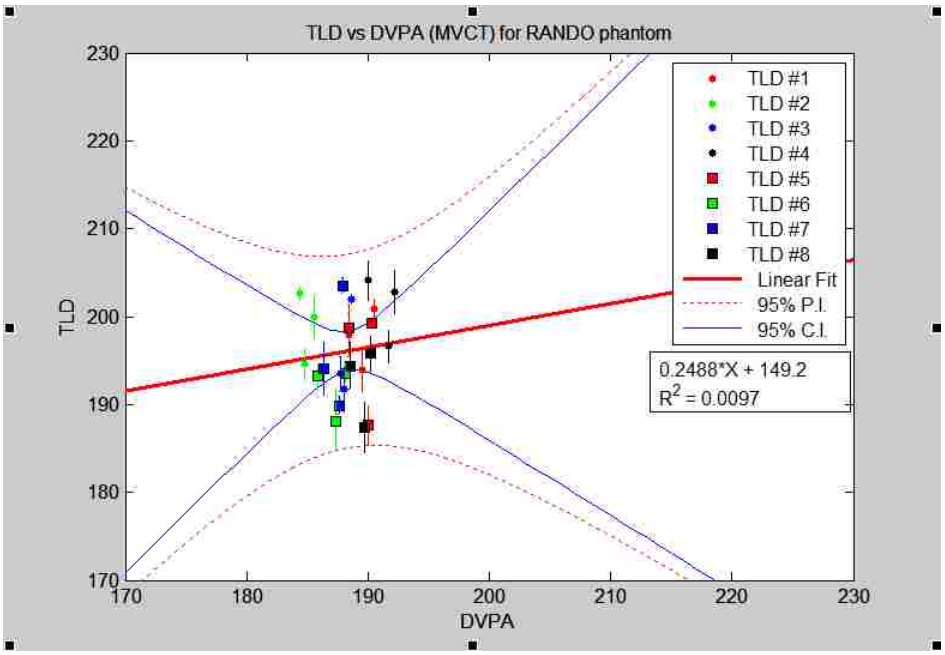

Figure 3-37: TLD doses vs. corresponding DVPA doses for the RANDO phantom organized by TLD location for DVPA doses calculated from the MVCT

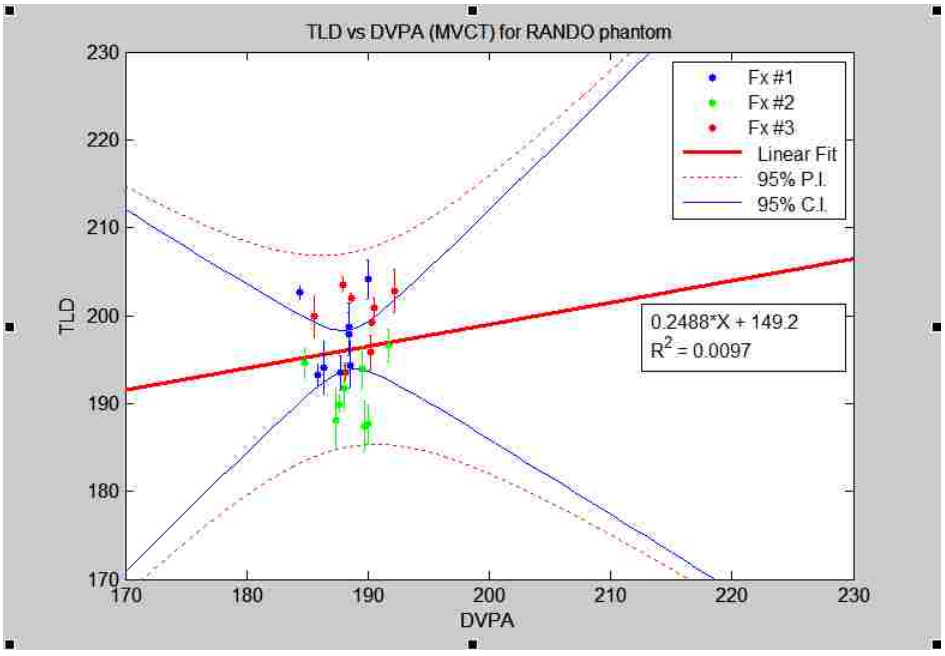

Figure 3-38: TLD doses vs. corresponding DVPA doses for the RANDO phantom organized by treatment fraction for DVPA doses calculated from the MVCT

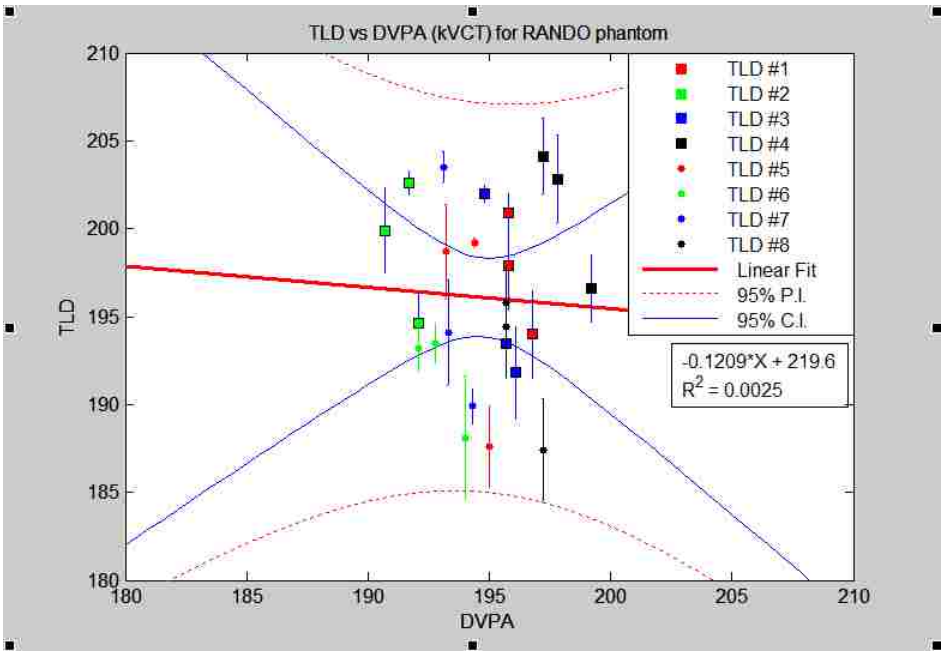

Figure 3-39: TLD doses vs. corresponding DVPA doses for the RANDO phantom organized by TLD location for DVPA doses calculated from the kVCT

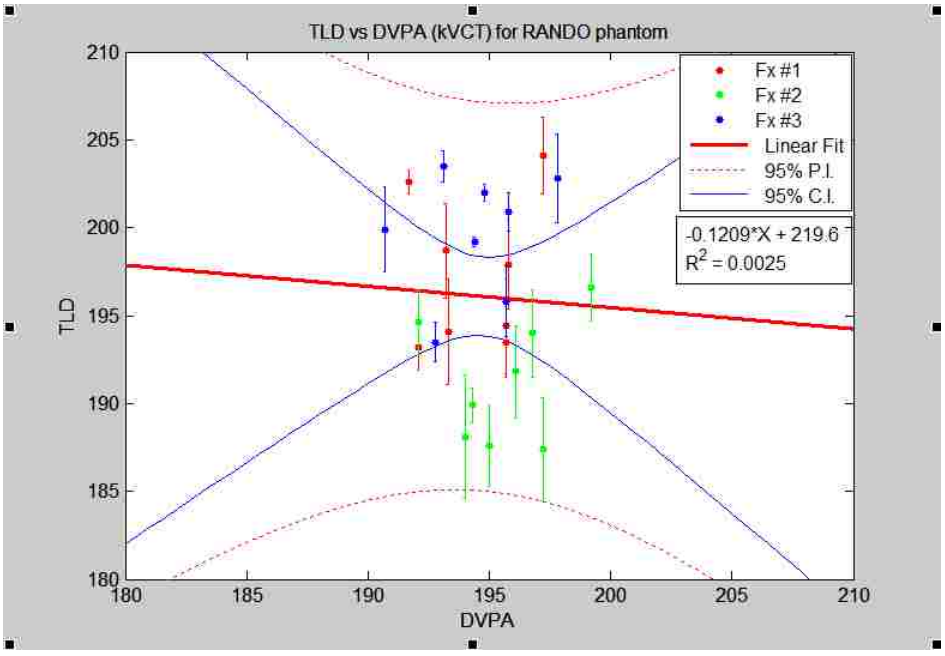

Figure 3-40: TLD doses vs. corresponding DVPA doses for the RANDO phantom organized by treatment fraction for DVPA doses calculated from the kVCT

The correlation between TLD doses and DVPA doses was weak for both cases where DVPA doses were calculated from either the MVCT or kVCT image sets. For the DVPA doses calculated from the kVCT there was a negative slope which is opposite of the ideal case. However, there was a limited number of data points used (24 total measurements), and more importantly the data is all clustered around similar dose values with random fluctuations in both the TLD and DVPA doses which causes the poor correlation. This was mostly to be expected since the planned doses were all relatively the same at approximately 200 cGy, and the variation of the doses was of the same order as the uncertainty in the dose values.

Chapter 4. Conclusions

I. Response to Hypothesis

The hypothesis tested in this work was that corresponding TomoTherapy DVPA calculated doses and patient/phantom in-vivo TLD doses would agree within 5% for 95% of data points and 10% for all data points.

This hypothesis is not true based on the following data: 66.3% (187 out of 282) of the patient TLD dose points agreed with corresponding DVPA calculated doses within 5% and 93.3% (263 out of 282) of the patient TLD dose points agreed with corresponding DVPA calculated doses within 10%. For the phantom irradiations where DVPA doses were calculated from the MVCT, 62.5% (15 out of 24) of the phantom TLD dose points agreed with corresponding DVPA calculated doses within 5%, while all 24 of the phantom TLD dose points agreed with corresponding DVPA calculated doses within 10%. For the phantom irradiations where DVPA doses were calculated from the kVCT, 87.5% (21 out of 24) of the phantom TLD dose points agreed with corresponding DVPA calculated doses within 5%, while all 24 of the phantom TLD dose points agreed with corresponding DVPA calculated doses within 10%.

II. Conclusions and Discussion

Despite the overall agreement of -3.2 ± 4.7% for the patient data comparison, the large number of comparisons that are outside of the 5% clinical acceptability criterion make the current database technique for delivery verification and dose reconstruction a poor candidate for the replacement of in-vivo TLD measurements at this time.

The phantom data comparison where DVPA doses were calculated with the MVCT image sets had an agreement of 3.9 ± 2.6%, but also had a large number of data points outside of

5% agreement. This is likely a result of an inaccurate IVDT causing a systematic shift in the dose calculations because when the DVPA doses were calculated with the kVCT image sets the agreement was 0.6 ± 2.9%. Also, nearly 90% of the relatively small number of data points compared within 5%. With the phantom study, where no interfraction or intrafraction motion is present in the treatment delivery, the largest source of error is probably from the TLD dose measurements with a range of uncertainty of approximately 3%.

Other possible reasons why the agreement between the TLD and reconstructed point doses suffered may be the that the dose calculation technique uses projection-by-projection calculations (where the 360° gantry rotation is broken into 51 discrete projections) and this method can lead to dose calculation inaccuracies near the surface especially when many oblique beamlets are being used [19]. Also, the calculation of radiological pathlength may suffer from voxelization artifacts near the surface when oblique beamlets are used as well [24]. Both of these inaccuracies will be inflated by patient motion.

Despite the fact that any motion variables were removed from the phantom study, there was still a similar amount of disagreement as the patient comparison when the DVPA doses were calculated with the MVCT image sets. When the kVCT image sets were used to calculate the DVPA doses the agreement increased dramatically with the percentage of points within 5% increasing by 25%. This indicates that an incorrect IVDT was used when using the MVCT image sets. With the increased agreement from using the kVCT for dose calculations, the remaining large source of error is in the TLD dose measurements, and the uncertainty from the TLD doses is on the order of the standard deviation seen in the DVPA dose vs. TLD dose percent difference comparisons.

III. Future Study

Currently, the dose reconstruction software uses a machine specific airscan scaled version of the "Gold Standard" database. Perhaps it would be useful to measure any possible differences between the scaled database and a database measured on the machine being used. Or to measure differences in the scaled database measurements over time based on machine fluctuations.

It may also be helpful to evaluate other treatment sites, possibly at depth, to see whether the inaccuracies mostly occur near the surface or throughout the entire dose profile. Using dose profiles and comparing them to film measurements may also be better than point dose comparisons with TLD to see whether distance to agreement measurements contribute to the dose comparisons. Ion chamber measurements are more precise than TLD measurements and could be used for point dose comparisons in place of TLD.

Finally, some amount of known setup shift should be applied to the phantom treatment to quantify the effect that patient motion has in the dose comparison procedure. If it can be seen that the DVPA recalculated doses are precise based on dosimeters other than TLD, and that the IVDT can be accurately modeled for dose computation, then intrafraction motion should be accurately taken into account in the dose calculations because they can be calculated using the known patient geometry from the MVCT images. However, any intrafraction motion will still cause a discrepancy.

References

1. Institute, N.C. *Comprehensive Cancer Information*. 2010 [cited 2011 June 20]; Available from: www.cancer.gov.

2. Dewar, J.A., *Postmastectomy radiotherapy.* Clin Oncol (R Coll Radiol), 2006. **18**(3): p. 185-90.

3. Recht, A. and S.B. Edge, *Evidence-based indications for postmastectomy irradiation.* Surg Clin North Am, 2003. **83**(4): p. 995-1013.

4. Overgaard, M., et al., *Postoperative radiotherapy in high-risk premenopausal women with breast cancer who receive adjuvant chemotherapy. Danish Breast Cancer Cooperative Group 82b Trial.* N Engl J Med, 1997. **337**(14): p. 949-55.

5. Overgaard, M., et al., *Postoperative radiotherapy in high-risk postmenopausal breast-cancer patients given adjuvant tamoxifen: Danish Breast Cancer Cooperative Group DBCG 82c randomised trial.* Lancet, 1999. **353**(9165): p. 1641-8.

6. *Adjuvant Therapy for Breast Cancer.* NIH Consensus Statement Online, 2000. **17**(4): p. 23.

7. *Lymph Nodes*. 2010 [cited 2010 November 29]; Available from: http://www.breastcancer.org/treatment/surgery/lymph_node_removal/lymph_nodes.jsp.

8. Kunkler, I., *Adjuvant chest wall radiotherapy for breast cancer: black, white and shades of grey.* Eur J Surg Oncol, 2010. **36**(4): p. 331-4.

9. Cheng, J.C., et al., *Locoregional recurrence in patients with one to three positive axillary nodes after mastectomy without adjuvant radiotherapy.* J Formos Med Assoc, 2000. **99**(10): p. 759-65.

10. Cheng, J.C., et al., *Locoregional failure of postmastectomy patients with 1-3 positive axillary lymph nodes without adjuvant radiotherapy.* Int J Radiat Oncol Biol Phys, 2002. **52**(4): p. 980-8.

11. Macdonald, S.M., et al., *Chest wall radiotherapy: middle ground for treatment of patients with one to three positive lymph nodes after mastectomy.* Int J Radiat Oncol Biol Phys, 2009. **75**(5): p. 1297-303.

12. Truong, P.T., et al., *Clinical practice guidelines for the care and treatment of breast cancer: 16. Locoregional post-mastectomy radiotherapy.* CMAJ, 2004. **170**(8): p. 1263-73.

13. Krueger, E.A., et al., *Potential gains for irradiation of chest wall and regional nodes with intensity modulated radiotherapy.* Int J Radiat Oncol Biol Phys, 2003. **56**(4): p. 1023-37.

14. Cheng, S.H., et al., *The benefit and risk of postmastectomy radiation therapy in patients with high-risk breast cancer.* Am J Clin Oncol, 1998. **21**(1): p. 12-7.

15. Pierce, L.J., et al., *Postmastectomy radiotherapy of the chest wall: dosimetric comparison of common techniques.* Int J Radiat Oncol Biol Phys, 2002. **52**(5): p. 1220-30.

16. Mackie, T.R., et al., *Tomotherapy: a new concept for the delivery of dynamic conformal radiotherapy.* Med Phys, 1993. **20**(6): p. 1709-19.

17. Welsh, J.S., et al., *Clinical implementation of adaptive helical tomotherapy: a unique approach to image-guided intensity modulated radiotherapy.* Technol Cancer Res Treat, 2006. **5**(5): p. 465-79.

18. Ruchala, K.J., et al., *Megavoltage CT on a tomotherapy system.* Phys Med Biol, 1999. **44**(10): p. 2597-621.

19. Cheek, D., et al., *Accuracy of TomoTherapy treatments for superficial target volumes.* Med Phys, 2008. **35**(8): p. 3565-73.

20. Khan, F.M., *The physics of radiation therapy*. 4th ed. 2010, Philadelphia: Lippincott Williams & Wilkins. x, 531, 30 p.

21. Ashenafi, M., et al., *Feasibility of postmastectomy treatment with helical TomoTherapy.* Int J Radiat Oncol Biol Phys, 2010. **77**(3): p. 836-42.

22. Ito, S., et al., *Verification of Calculated Skin Doses in Postmastectomy Helical Tomotherapy.* Int J Radiat Oncol Biol Phys, 2011.

23. Fenwick, J.D., et al., *Quality assurance of a helical tomotherapy machine.* Phys Med Biol, 2004. **49**(13): p. 2933-53.

24. Kapatoes, J.M., et al., *A feasible method for clinical delivery verification and dose reconstruction in tomotherapy.* Med Phys, 2001. **28**(4): p. 528-42.

25. Kapatoes, J.M., et al., *Delivery verification in sequential and helical tomotherapy.* Phys Med Biol, 1999. **44**(7): p. 1815-41.

26. Kapatoes, J.M., et al., *On the accuracy and effectiveness of dose reconstruction for tomotherapy.* Phys Med Biol, 2001. **46**(4): p. 943-66.

27. Hesston, R., *Dosimetric evaluation of a delivery verification and dose reconstruction method for helical tomotherapy*, in *Department of Physics and Astronomy*. 2009, Louisiana State University: Baton Rouge. p. 1-98.

28. Kutcher, G.J., et al., *Comprehensive QA for radiation oncology: report of AAPM Radiation Therapy Committee Task Group 40.* Med Phys, 1994. **21**(4): p. 581-618.

Vita

Matthew Roberts was born in Cedar Rapids, Iowa, in June of 1985, the son of Joan and Johnie Roberts. He graduated from Springville High School in 2004, and then went on to obtain his Bachelor of Arts degree with majors in physics and computer science and a minor in mathematics from Coe College in 2008. In August of 2008, he entered the medical physics graduate program at Louisiana State University.